

LLM-to-Phy3D: Physically Conform Online 3D Object Generation with LLMs

Melvin Wong^{1*} Yueming Lyu² Thiago Rios³ Stefan Menzel³ Yew-Soon Ong^{1,2*}

¹College of Computing & Data Science, Nanyang Technological University, Singapore

²Centre for Frontier AI Research, Agency for Science, Technology and Research, Singapore

³Honda Research Institute Europe (HRI-EU), Offenbach am Main, Germany

{wong1357, asysong}@ntu.edu.sg
Lyu_Yueming@cfar.a-star.edu.sg
{thiago.rios, stefan.menzel}@honda-ri.de

Abstract

The emergence of generative artificial intelligence (GenAI) and large language models (LLMs) has revolutionized the landscape of digital content creation in different modalities. However, its potential use in Physical AI for engineering design, where the production of physically viable artifacts is paramount, remains vastly underexplored. The absence of physical knowledge in existing LLM-to-3D models often results in outputs detached from real-world physical constraints. To address this gap, we introduce LLM-to-Phy3D, a physically conform online 3D object generation that enables existing LLM-to-3D models to produce physically conforming 3D objects on the fly. LLM-to-Phy3D introduces a novel online black-box refinement loop that empowers large language models (LLMs) through synergistic visual and physics-based evaluations. By delivering directional feedback in an iterative refinement process, LLM-to-Phy3D actively drives the discovery of prompts that yield 3D artifacts with enhanced physical performance and greater geometric novelty relative to reference objects, marking a substantial contribution to AI-driven generative design. Systematic evaluations of LLM-to-Phy3D, supported by ablation studies in vehicle design optimization, reveal various LLM improvements gained by 4.5% to 106.7% in producing physically conform target domain 3D designs over conventional LLM-to-3D models. The encouraging results suggest the potential general use of LLM-to-Phy3D in Physical AI for scientific and engineering applications.

1 Introduction

Remarkable advancements in generative artificial intelligence (GenAI) and large language models (LLMs) have opened up new research opportunities, focusing primarily on the creation of high-fidelity digital artifacts that faithfully align with user preferences through tailored prompts. This has led to a surge in broad applications including text-to- X generation that produces digital artifacts of different modalities (e.g., text, image, or 3D) conditioned on textual prompts (Dong et al. [2022], Bie et al. [2025], Lee et al. [2024]).

Among those applications, text-to-3D object generation has attracted increasing attention due to its success and potential to democratize 3D content creation, accelerate design workflows, and leverage

*corresponding authors



Figure 1: Most representative vehicles generated with various conventional LLM-to-3D models using LLM-generated prompts (left) and physically conforming novel vehicles generated with LLM-to-Phy3D (right).

the capabilities of emerging multimodal foundation models (Lee et al. [2024]). One main problem of 3D object generation is automating the design process while enabling the synthesis of novel and diverse shapes (Li et al. [2024]). Several works introduce text-to-3D models that can generate the parameters of implicit functions for rendering textured meshes and neural radiance fields (Li et al. [2023b], Jun and Nichol [2023]). This enables the synthesis of diverse 3D shapes in a target domain from a single text prompt. Xiang et al. [2024] proposed a unified structured latent representation that expands the generation of outputs to the 3D Gaussian format and improves the quality of generated artifacts. Wang et al. [2024] attempted to unify the spatial textual knowledge in LLMs with 3D information to improve mesh understanding, enabling the generation of simple polygonal meshes in textual format.

While these advancements led to the proliferation of digital media applications, there is a notable lack of progress in advancing 3D object generation in Physical AI for engineering design, where the production of physically viable artifacts is paramount (Banerjee et al. [2024], Liu et al. [2025]). One major challenge we observed is the generation of objects that satisfy physical constraints. 3D vehicles generated from conventional text-to-3D models without physical knowledge (Figure 1 (Left Group) and Figure 2 (a)) while aesthetically pleasing, have limited efficacy in both the real physical world and its digital twin as compared to ones generated with these constraints (Figure 1 (Right Group) and Figure 2 (b)). Notable work attempts to incorporate such constraints in GenAI models, focusing on enforcing the generation of a targeted object shape to comply with physical laws (Xu et al. [2025]). However, due to confidentiality concerns and prohibitive data generation costs, the scarcity of large-scale, high-quality engineering data poses difficulties in scaling and generalizing such techniques for text-to-3D generation. In contrast, black-box techniques can overcome such difficulties, enabling existing GenAI models to generate novel artifacts that conform to targeted physical constraints. Pioneering research studies that investigate this approach in engineering design optimization, where preliminary results, particularly in enhancing aerodynamic performance while satisfying domain constraints (Rios et al. [2023], Wong et al. [2024]), encourage progress and interest. These efforts motivate for GenAI with language models to narrow the gap between digital innovation and functional applicability, driving progress in Physical AI for engineering design. However, these methods focus on improving conventional optimization strategies. To date, the feasibility of LLMs in producing 3D artifacts that conform to physics for engineering design remains vastly underexplored.

To this end, we introduce *LLM-to-Phy3D*, a novel physically conform online 3D object generation with LLMs. Central to LLM-to-Phy3D is its unique online black-box iterative refinement framework that adaptively steers the LLM to find textual prompts that yield physically plausible 3D artifacts with high geometric novelty. The framework starts with 3D artifacts generated with randomly sampled LLM-generated prompts. Subsequently, LLM-to-Phy3D quantifies the physical performance, target domain alignment, and geometric novelty of 3D artifacts with visual and physics-based evaluations, which serve as surrogate indicators for a non-differentiable black-box objective. An iteration of LLM-to-Phy3D ends with a selection process that picks the best-performing LLM-generated prompts as exemplars for the LLM to learn the relationship between its prompts and the generated 3D artifacts that resulted in the quantified score, enabling the LLM to improve its performance in the next iteration. This selection pressure mechanism not only ensures constant space complexity but, more importantly,

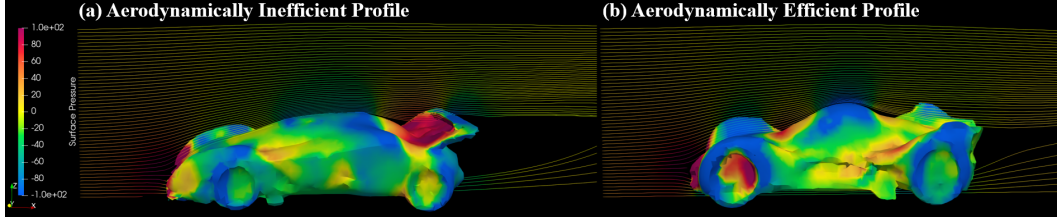


Figure 2: Aerodynamic Visualization of two vehicles generated (a) without considering physical constraints and (b) with physical constraints. Vehicle shape has a direct impact on the aerodynamic (drag) performance. Some aerodynamically efficient (low drag) characteristics include attached streamline flow from the front to the rear, and small pressure differences between the front and rear. In contrast, an aerodynamically inefficient (high drag) vehicle exhibits opposing characteristics, including separated streamline flow and pronounced pressure differences.

achieves the desired generation characteristics with directional feedback (Shimabucoro et al. [2024], Nie et al. [2023]) that steers the LLM to produce physically conforming target domain 3D artifacts.

Moreover, generation issues, such as hallucinations (Jesson et al. [2024]), produce 3D artifacts with shapes that are not within the target domain yet satisfy the physical constraints. Visual evaluations can not only effectively identify and penalize irrelevant shapes but also reward novel ones. While existing foundation vision models can assess such artifacts from 2D rendered views with a high degree of accuracy (Li et al. [2023a], Tan and Le [2019]), the projection of 3D artifacts onto 2D can cause significant geometric distortions in the surface topology that degrade the model performance. To address such issues, we propose conducting the physical light simulation under orthographic projection (Parker et al. [2010]) to capture the precise surface topology of 3D artifacts and minimize geometric distortions. This single visual representation serves the dual purpose of object recognition and geometric novelty quantification with respect to reference objects.

To demonstrate the efficacy of LLM-to-Phy3D against conventional LLM-to-3D methods, we conduct experiments on a test scenario that mimics real-world engineering design optimization. Starting from initial LLM-generated prompts that yield 3D artifacts with significant variation in physical performance, we demonstrate that all LLMs in our experiments are able to improve the quality of its generated prompts, leading to significant improvements in producing physically conforming novel 3D artifacts with better realism than the ones generated with conventional text-to-3D models. To summarize, the contributions of this paper are as follows:

- We introduce *LLM-to-Phy3D*, a novel physically conform online 3D object generation with LLMs, for actively steering the LLM to produce physically conforming novel 3D objects. LLM-to-Phy3D enables the LLM to find effective prompts by providing physical knowledge through directional feedback. This allows the LLM to learn the association between its generated prompts and the quality of 3D artifacts generated with its these prompts.
- LLM-to-Phy3D captures the precise surface topology and visual characteristics of 3D artifacts through physical light simulation with orthographic projection in a single visual representation for object recognition and geometric novelty quantification with respect to reference objects. The technique minimizes geometric distortion, ensuring the rendered surface topology conforms to scientific and engineering requirements.
- Visual and physics-based evaluations are introduced to quantify the quality of 3D-generated artifacts based on its physical performance and geometric novelty. These evaluations contribute to the search objective, enabling the selection of physically conforming ones as exemplars for the LLM to learn from in the next iteration.
- In contrast to existing LLM benchmark approaches, which tailor meta-prompts for different LLMs, we evaluate the performance of four state-of-the-art LLMs with the same standardized meta-prompt to ensure a fair comparison of search performance. Systematic evaluations of LLM-to-Phy3D, along with ablation studies in aerodynamic vehicle design optimization tasks, reveal various LLM improvements gained by 4.5% to 106.7% in producing physically conforming target domain 3D designs, indicating the broader potential of the framework in Physical AI for science and engineering applications.

2 Preliminaries

In this paper, we articulate the physical viability of 3D objects in the context of, but not limited to, the automotive aerodynamics design scenario. As such, we introduce in this section the key fundamental concepts in representing and quantifying the novelty and quality of 3D objects.

Surface Topology Representation for Object Recognition and Geometric Novelty Quantification:

In many computer vision and computer graphics applications, the semantic meaning and visual features of a 3D object are defined based on the object’s surface topology (Rothwell et al. [1996], Montagnat et al. [2001], Pulli and Shapiro [2000]). This topology information can be captured with the illumination of the surface through a physical light simulation (Parker et al. [2010]), which replicates physical light rays reflecting and refracting from the surface and projects onto a camera plane. Assuming camera orthographic projection, given a set of all intersection points \mathbf{Z}_c in a fixed camera viewpoint c of a 3D-object \mathbf{x} , the surface topology of the rendered R multi-view is defined as:

$$g(\mathbf{x}) = \{\mathbf{X} = \{I(\mathbf{z}) \mid \forall \mathbf{z} \in \mathbf{Z}_c\} \mid \forall c \in \{1, \dots, R\}\}, \quad (1)$$

where \mathbf{X} is a rendered view image of \mathbf{x} consisting of the illumination (or shading) from multiple light rays intersecting at different surface point \mathbf{z} by $I(\cdot)$. In this paper, we compare the multi-view of generated and reference 3D objects to minimize inaccuracies in determining the region of geometric novelty due to surface topology distortion caused by indirect illumination. Details of this illumination process (Dutre et al. [2018]) are discussed in the supplementary background Section A.1.2.

Aerodynamics Computation for Physical Performance Quantification: For automotive aerodynamics, the drag and lift characteristics of a vehicle are of prime interest. These characteristics can be quantified with a physics simulator (or surrogate) G where the vehicle is subject to fluid flow conditions, such as steady or unsteady air streams, replicating real-world aerodynamic environments. The fluid particles interacting with the surface of the vehicle create viscous forces and pressures in the flow direction that drag or lift the vehicle body. Assuming the particles are travelling along the x -axis, given the projected area of the vehicle ($A_{\text{projected}}$), the drag and lift scores are defined as:

$$G_{\text{fluid_forces}}(\mathbf{x}, \mathcal{F}) \approx \frac{\mathcal{F}(\mathbf{x})}{2\rho_{\infty} \|\mathbf{u}_{\infty}\|_2^2 \cdot A_{\text{projected}}}, \quad (2)$$

$$\bar{C}_{\text{lift}}(\mathbf{x}) = G_{\text{fluid_forces}}(\mathbf{x}, \mathcal{F}_z), \quad \bar{C}_{\text{drag}}(\mathbf{x}) = G_{\text{fluid_forces}}(\mathbf{x}, \mathcal{F}_x),$$

where ρ_{∞} is the freestream ambient density of the fluid, and \mathbf{u}_{∞} is the freestream velocity vector. Here, $\mathcal{F}(\cdot)$ computes the integral forces acting on the surface with $\mathcal{F}_x(\cdot)$ considering the forces along the x -axis only while $\mathcal{F}_z(\cdot)$ take into account forces along the z -axis only. Note that the drag and lift coefficients (\bar{C}_{drag} and \bar{C}_{lift}) are usually computed in a dimensionless and normalized form. Background information on the fluid dynamics computation (Lomax et al. [2001]) to compute the drag and lift is presented in the supplementary background Section A.1.1.

3 Method: LLM-to-Phy3D

We first present the LLM-to-Phy3D framework, followed by detailed discussions of the key components of the framework.

3.1 Online Blackbox Iterative Refinement Framework

Without loss of generality, let \mathcal{P} denote a space of textual prompts and \mathcal{X} denote a space of 3D objects. Given any 3D object $\mathbf{x} \in \mathcal{X}$, we assume a text-to-3D GenAI model (p_{t3d}) that generate new 3D objects conditioned on a textual prompt. Moreover, given any prompt $\mathbf{m} \in \mathcal{P}$, we also assume the presence of an LLM-based optimizer (p_{llm}) that can iteratively generate new prompts based on the domain of interest \mathcal{S} and a meta-prompt \mathbb{M} , and can be adaptively guided using exemplars consisting of prompts paired with its performance in generating high-quality 3D objects. As such, given a set \mathbf{Y} of reference 3D objects, the search goal is to find novel 3D artifacts that satisfy physical and domain constraints:

$$\begin{aligned} \min_{\mathbf{m} \in \mathcal{P}} : & \quad \mathbb{E}_{\mathbf{x} \sim p_{\text{t3d}}(\mathbf{x} \mid \mathbf{m})} [f_{\text{physical}}(\mathbf{x}) + f_{\text{domain}}(g(\mathbf{x}), \mathcal{S}) - \beta F_{\text{novelty}}(\mathbf{x}, \mathbf{Y})] \\ \text{s.t. } & \quad Q(\mathbf{m}, \mathcal{S}) \leq \epsilon, \\ & \quad \underline{c} \leq f_{\text{physical}}(\mathbf{x}) \leq \bar{c}, \end{aligned} \quad (3)$$

where $Q(\cdot, \cdot)$ is a function that filters infeasible LLM-generated prompts, due to generation failure scenarios (e.g. LLM hallucination), which are semantically distant to the domain of interest \mathcal{S} by ϵ . Moreover, $\underline{c} > 0.0$ and $\bar{c} < 1.0$ define the boundary that any 3D generated artifact in the target

domain can realistically achieve in the real world, effectively filtering infeasible ones such as the non-conforming or non-watertight with object’s surfaces are not fully closed. The first term ranks generated artifacts with better physical performance, scoring higher than impractical ones. Among those that satisfy the physical constraint, generated artifacts less resembling \mathcal{S} are penalized in the second term, demoting its position for such artifacts. Finally, the third term rewards artifacts with high geometric novelty with respect to the target domain, promoting the positions. This term is weighted with a β parameter to balance the novelty score with the physical score. These three terms work in synergy to provide the LLM with effective feedback on the quality of generated artifacts, ensuring that the better-quality candidates serve as exemplars to the LLM in subsequent iterations.

Algorithm 1 describes the mechanics of the framework. Given a user domain \mathcal{S} and design specifications \mathcal{C} , LLM-to-Phy3D initializes the LLM (p_{llm}) with the search task. Our proposed method then samples prompts from the LLM to produce the corresponding 3D artifacts from the text-to-3D generative model p_{t3d} . The generated 3D artifacts are evaluated against the specifications to determine the scores. These scores are then combined with the LLM-generated prompts to serve as exemplars for the LLM to learn and re-attempt to create new prompts that can yield better-performing candidates. These candidates are evaluated and, together with the ones generated in the last iteration, undergo a selection process. This process selects the better-performing candidate from randomly paired candidates to form an exemplar set of N candidates for the next iteration (Line 7 in Algorithm 1), ensuring constant space complexity throughout the search. Moreover, the exemplar set serves as directional feedback, allowing it to learn the association between the prompt and the quality of the 3D object and find more effective prompts that steer towards the optimal. LLM-to-Phy3D iterates until the terminating condition is satisfied.

Algorithm 1 LLM-to-Phy3D

Input: \mathbb{M} meta prompt, \mathcal{S} domain specifications, and \mathcal{C} design specifications, batch-size N

Output: Designs Set $\mathcal{D}_{\text{step}}$

```

1: step  $\leftarrow$  0
2:  $\mathcal{D}_{\text{step}} \leftarrow \{(\mathbf{m}_i, \mathbf{x}_i) \mid \mathbf{m}_i \sim p_{\text{llm}}(\mathbf{m}_i \mid \mathbb{M}, \mathcal{S}), \mathbf{x}_i \sim p_{\text{t3d}}(\mathbf{x}_i \mid \mathbf{m}_i)\} \quad \forall i \in \{1, \dots, N\}$ 
3: Evaluate  $\mathcal{D}_{\text{step}}$  against  $\mathcal{C}$  and  $\mathcal{S}$  based on Equation (5), (4), (7), and (3)
4: while non-terminating condition do
5:    $\mathcal{D}_{\text{candidates}} \leftarrow \{(\mathbf{m}_i, \mathbf{x}_i) \mid \mathbf{m}_i \sim p_{\text{llm}}(\mathbf{m}_i \mid \mathbb{M}, \mathcal{S}, \mathcal{D}_{\text{step}}), \mathbf{x}_i \sim p_{\text{t3d}}(\mathbf{x}_i \mid \mathbf{m}_i)\} \quad \forall i \in \{1, \dots, N\}$ 
6:   Evaluate  $\mathcal{D}_{\text{candidates}}$  against  $\mathcal{C}$  and  $\mathcal{S}$  based on Equation (5), (4), (7), and (3)
7:    $\mathcal{D}_{\text{step}+1} \leftarrow \text{select\_N\_candidates}(\mathcal{D}_{\text{candidates}} \cup \mathcal{D}_{\text{step}})$ 
8:   step  $\leftarrow$  step + 1
9: end while

```

3.2 Quality of 3D Generated Objects

We quantify the quality of a 3D-generated object \mathbf{x} with the following measures:

(a) Physical Constraint with Physical Alignment Measure: This measure assesses the performance of 3D-generated objects under various physics conditions, governed by the natural physical laws. Here, we provide an instantiation of this measure in the context of fluid dynamics (Lomax et al. [2001]). As such, the physical alignment measure is defined as follows:

$$f_{\text{physical}}(\mathbf{x}, \mathcal{F}) = [\min(\max(G(\mathbf{x}, \mathcal{F}), a), b) - a] / (b - a), \quad (4)$$

where a physics simulator (or surrogate) $G(\cdot, \cdot)$, such as a Computational Fluid Dynamics (CFD) solver (Zawawi et al. [2018]), computes the physical performance of the 3D generated artifact \mathbf{x} .

(b) Domain Constraint with Domain Alignment Measure: Given a user-defined domain specification \mathcal{S} and multi-view images $g(\mathbf{x})$ of the 3D object \mathbf{x} , we measure the degree of alignment between the object and target domain with the following measure:

$$s_1 = H_{\text{vlm}}(g(\mathbf{x}), \mathcal{S}), \quad s_2 = H_{\text{vlm}}(g(\mathbf{x}), \neg\mathcal{S}), \quad (5)$$

$$f_{\text{domain}}(g(\mathbf{x}), \mathcal{S}, \Gamma) = e^{s_1/\Gamma} / (e^{s_1/\Gamma} + e^{s_2/\Gamma}),$$

where Γ is the temperature hyperparameter that controls the discriminative strength between the positive and negative pairs. Here, we assess the likelihood that a 3D object is within the target domain \mathcal{S} with a Visual-Language Model $H_{\text{vlm}}(\cdot, \cdot)$ that sets $\Gamma = 0.01$. More detailed background information is presented in the supplementary section A.1.3.

(c) Geometric Novelty Measure: This measure detects and localizes the regions of geometric novelty by comparing the surface topology of a 3D-generated object with a reference object. The surface topology differences with the reference object indicate regions of geometric novelty that contribute to the improvement or degradation of the overall physical performance f_{physical} . Here, we instantiate this measure in the context of physical light simulation (Parker et al. [2010]), capturing the precise surface topology of a 3D object. As such, given a 3D-generated object \mathbf{x} and a target object \mathbf{y} in the conventional set, the measure compares images of the same rendered view, defined as follows:

$$\begin{aligned} s_3 &= \sum_{i=1}^R \|\mathbf{M} \odot g(\mathbf{y})^{[i]} - \mathbf{M} \odot g(\mathbf{x})^{[i]}\|_2^2, \\ s_4 &= \sum_{i=1}^R \sum_{j=1}^J \|h_j(\mathbf{M} \odot g(\mathbf{y})^{[i]}) - h_j(\mathbf{M} \odot g(\mathbf{x})^{[i]})\|_2^2, \\ f_{\text{novelty}}(\mathbf{x}, \mathbf{y}) &= \frac{\gamma(g(\mathbf{x}), g(\mathbf{y}))(s_3 + s_4)}{\|\mathbf{M}\|_1}, \end{aligned} \quad (6)$$

where \odot denotes the element-wise product, R is the number of rendered views, $g(\cdot)^{[i]}$ provides the i -th rendered view of a 3D object, and \mathbf{M} is a mask matrix for indicating the regions of interest to compare the surface topology. The first term s_3 compares the same rendered view image between the 3D-generated and target object at the pixel level. The second term s_4 compares various visual feature maps with a pre-trained image feature extractor $h_j(\cdot)$, which extracts specific features at the j -th level of image abstraction. On a separate note, the measure score is weighted with $\gamma(\cdot, \cdot)$ to ensure the relevance of the 3D-generated novelty with respect to the target domain. This allows impractical 3D-generated objects that have no resemblance to the target domain to be ranked lower than the practical ones. Details of this weighted function $\gamma(\cdot, \cdot)$ are discussed in the supplementary section A.1.3. In addition, the f_{novelty} is scale invariant by normalizing with the number of pixels considered in the regions of interest $\|\mathbf{M}\|_1$. Furthermore, if a set \mathbf{Y} of reference objects is provided, the reference object with the least geometric novelty with respect to \mathbf{x} is selected as the representative novelty of the set and is defined as:

$$F_{\text{novelty}}(\mathbf{x}, \mathbf{Y}) = \min_{k \in \{1, \dots, K\}} \{f_{\text{novelty}}(\mathbf{x}, \mathbf{y}_k) \mid \mathbf{y}_k \in \mathbf{Y}\}. \quad (7)$$

3.3 Meta Prompt Design

A set of instructions (or meta-prompt) is designed for the LLM to function as an effective optimizer. Specifically, a role description highlights the search task the LLM operates and the goal (or objective) it needs to solve. LLM is provided with target domain knowledge for generating domain-specific prompts, effectively constraining the generation of 3D objects within this domain. To this end, we instruct the LLM to complete the following prompt template, $\mathcal{M} = \text{“A } \langle \mathcal{S} \rangle \text{ in the shape of”}$, where \mathcal{S} is user specified domain specification. Lastly, for the LLM to improve its generative performance, we provide the LLM with feedback by presenting previously LLM-generated prompts with its evaluated scores as exemplars for the LLM to reflect on and learn from. This in-context learning approach improves the likelihood that the LLM generates more effective prompts than its previous iteration.

4 Experiments

4.1 Setup and Evaluation

We demonstrate the efficacy of LLM-to-Phy3D with experiments set up to solve an engineering design optimization problem. The problem is designed to find novel cars with aerodynamically efficient (low drag) body shapes. As such, the target domain \mathcal{S} is set as “Car” and we design the meta prompt for the problem with the search goal of minimizing the aerodynamic drag \bar{C}_{drag} in f_{physical} (see Figure 9 in the supplementary section for an example of the meta prompt). In addition, we bound the drag scores within $a = -1.0$ and $b = 1.0$ in Equation (4) and normalized. Moreover, we set β accordingly to only reward novel vehicles with better aerodynamic drag performance than a set of reference objects $\mathbf{Y} = \{\mathbf{y}_1, \dots, \mathbf{y}_Q\}$. Specifically, we first generate reference objects in \mathbf{Y} with the text-to-3D generative model in the test scope conditioned on “A Car”, and then determine the physical performance of each object. Subsequently, we compute the physical performance standard deviation $\hat{\sigma}$ and mean $\hat{\mu}$ of the set \mathbf{Y} for instantiating the hyperparameter as $\beta = e^{-(\hat{\mu}/\hat{\sigma})}$. We employ CFD physics simulation

with OpenFoam (Weller et al. [1998]) to obtain the physical performance aerodynamic scores. In addition, to generate the feature maps in Equation (6), we utilize the EfficientNet model (Tan and Le [2019]). Details of how the feature maps are utilized are discussed in the supplementary material Section A.1.3. On a separate note, we employ the Nvidia ray tracing engine OPTIX (Parker et al. [2010]) to capture and render the precise surface topology of 3D objects.

Our proposed method is compared against four different baseline LLM-to-3D methods. We select four LLMs - *GPT-3.5 Turbo*, *GPT-4o Mini*, *Gemini 2.0 Flash Lite*, and *Mistral 3.1 Small*, to compare based on its capabilities in following the designed meta-prompts and creating feasible prompts throughout the iterations in a single experiment run. As these LLMs require a text-to-3D generative model to produce 3D artifacts, we select *Shap-E* and *Trellis* models. For these baseline LLM-to-3D methods, we established a standard meta prompt “*Create a prompt that starts with \mathcal{M} and ends with a full stop.*”, where \mathcal{M} is the prompt template introduced in Section 3.3. Moreover, the temperature of the LLMs is set in a range that allows it to produce viable and diverse prompts. Also, for consistency, we adhere to the same temperature range for these LLMs, unless notable hallucination issues result in a significant degradation of the LLM’s ability to follow the instructions. Detailed specifications of these models are recorded in the supplementary section Table 3 and Table 4. Furthermore, we compare LLM-to-Phy3D against the baseline methods in terms of its ability to produce physically conforming target domain 3D artifacts. Specifically, given the target domain \mathcal{S} and set \mathcal{D} of all 3D artifacts generated with a method in a single experiment run, we define the domain and physical alignment rating (*DPAR*) of a method of interest as:

$$DPAR(\mathcal{D}, \mathcal{S}) = \mathbb{E}_{\mathbf{x} \in \mathcal{D}} [f_{\text{domain}}(g(\mathbf{x}), \mathcal{S}) / f_{\text{physical}}(\mathbf{x})],$$

where the higher the rating, the better the method in its ability to produce physically conforming target domain artifacts. For fair comparison, we ensure that the number of generated outputs in a baseline method and our proposed method is the same throughout the iterations (see supplementary section A.3 for more details). Furthermore, our proposed method and the baseline use the same LLM temperature ranges.

4.2 Results and Discussions

Based on the experiment results, the baseline models often generate vehicles that exhibit aesthetically pleasing shapes or resemble conventional vehicle body shapes (as observed in some of the most representative examples on the left group of Figure 1). In contrast to these vehicles, LLM-to-Phy3D found novel vehicles that are not only visually creative but also satisfy the physical and target domain constraints (presented in the right group of the same figure). This observation is evident in the benchmark with *DPAR* (Table 1), where our proposed method consistently outperforms the baselines by a margin of 4.46% to 106.74%. This varying resulting margin of LLM-to-Phy3D is the result of the performance of each LLM in learning the association between the quality of 3D artifacts and its LLM-generated prompts, and predicting the best possible prompts that yield better quality outputs.

As presented in Figure 3, *GPT-4o-mini* and *GPT-3.5-Turbo* can learn more proficiently than other LLMs of interest, resulting in convergence in less than 10 steps. On the other hand, while *Gemini 2.0 Flash Lite* is capable of producing diverse and creative prompts, we observe it requires more time to overcome the generation issues in *Shap-E* (Figure 3(a)) where the text-to-3D model is less adhering to the LLM-generated prompts. We also noticed that *Mistral 3.1 small* struggles to learn the association between its generated prompt and the evaluated score, hindering its performance in producing effective textual prompts. While still being able to find physically conforming and more novel 3D vehicles, the limitations observed in *Gemini 2.0 Flash Lite* and *Mistral 3.1 small* resulted in minimal variation of the generated prompts.

Table 1: Comparison of LLM-to-Phy3D and Baselines *DPAR* in Producing Physically Conform Target Domain 3D Artifacts

Text-to-3D Model / LLM	Shap-E			Trellis		
	Baseline	Ours	Improvement	Baseline	Ours	Improvement
Mistral 3.1 Small	0.8350	0.9557	+14.46%	0.8131	0.8494	+4.46%
GPT 3.5	0.8972	0.9637	+7.41%	0.8562	0.9531	+11.32%
GPT 4o Mini	0.6891	1.0000	+45.12%	0.6139	1.0000	+62.89%
Gemini 2.0 Lite	0.7697	0.9173	+19.18%	0.4660	0.9634	+106.74%

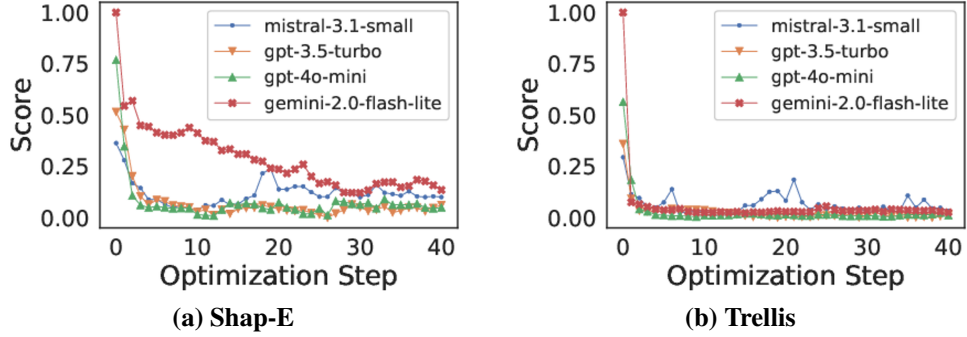


Figure 3: Search optimization score (Equation 3) of LLM-to-Phy3D with different LLM and text-to-3D generative models combinations.

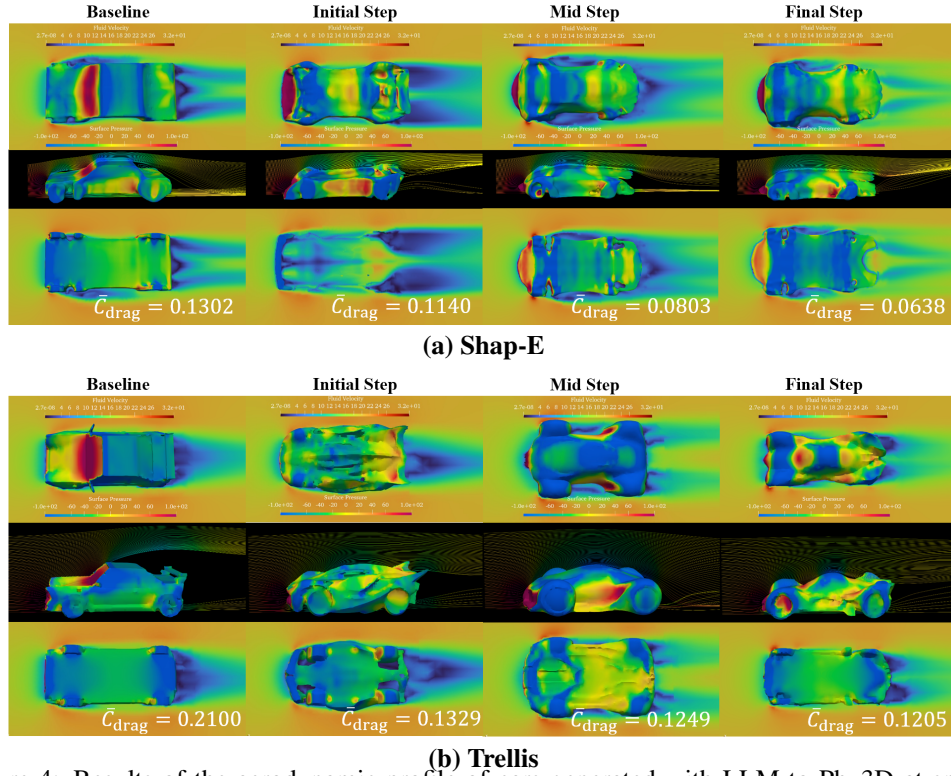


Figure 4: Results of the aerodynamic profile of cars generated with LLM-to-Phy3D at specific iterations and compared with a representative car generated with the best baseline LLM-to-3D method. Note that the lower the drag, the better the physical performance of the car.

By analyzing the aerodynamic performance of the generated 3D shapes (Figure 4), our findings reveal that the initialization step produces 3D-generated cars with shapes that yield high surface pressure at the car front and sides. This increases the aerodynamic drag force and decreases the performance. These resulting artifacts have similar aerodynamic issues to the baseline samples, as the LLMs generate textual prompts without prior knowledge of the physics. After introducing prior knowledge and selecting effective textual prompts that result in better physically conforming 3D artifacts, the generated 3D artifacts possess shapes that lead to lower aerodynamic performance indicators, such as a reduced pressure difference or smaller projected area.

We conducted several ablation studies to examine the effect of each term in the objective function. We noticed that using physical constraint f_{physical} only, the search favors malformed or highly fragmented

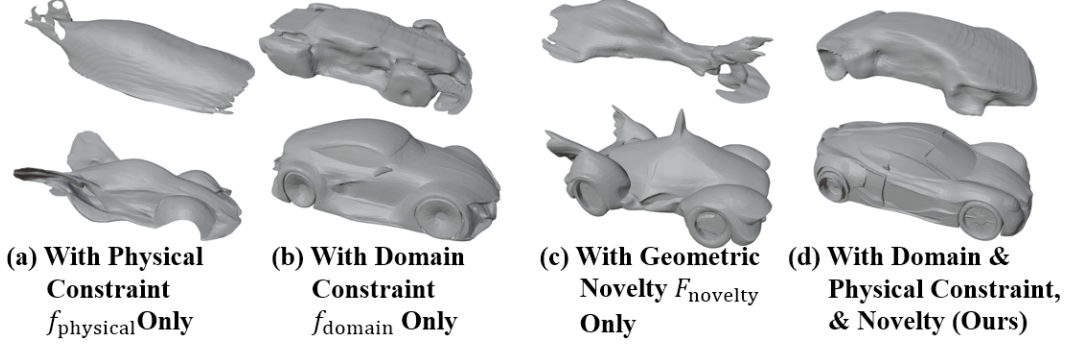


Figure 5: Ablation Studies on the effectiveness of different terms in the objective function on generating 3D artifacts (Top Row: LLM with Shap-E, Bottom Row: LLM with Trellis).

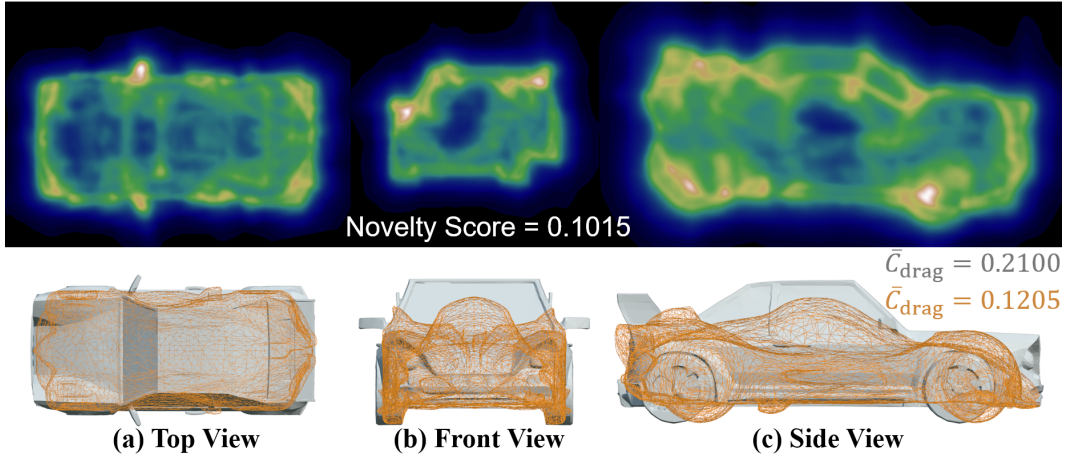


Figure 6: Example of geometric novelty between a reference car (in grey solids) and a car generated with LLM-to-Phy3D (in orange wireframe). The novelty heatmaps presented in the top row are the multi-view results of $F_{\text{novelty}}(\cdot)$, which highlight the regions contributing to the geometric novelty score of the generated car compared with the target one. Multiple views (bottom row) of the generated car overlay on top of the target car show regions corresponding to the contrasting body shapes attributed to the difference in aerodynamic performance.

cars (Figure 5 (a)) that registered better drag performance than complete generated cars. This degrades over time the overall performance of the framework as LLM learns the false positives, leading to an incorrect association of prompts with the cars, which results in shapes that yield poorer drag performance. On a separate note, the search process adhering to the target domain constraint f_{domain} only can lead to artifacts that visually highly resemble the reference cars of varying physical performance (Figure 5 (b)). With geometric novelty F_{novelty} only, on the other hand, LLMs found textual prompts that yield cars with highly unconventional or fragmented shapes that have high novelty but are impractical (Figure 5 (c)). By combining all three terms as a weighted sum in the objective function, LLM-to-Phy3D can effectively produce novel 3D artifacts that satisfy the physical and domain constraints (Figure 5 (d)).

Figure 6 reveals the highlighted visual features indicating the geometric novelty between a reference car and a car generated with LLM-to-Phy3D. In the top row heatmap images in the figure, the geometric differences between the surfaces of a 3D-generated car and a reference one are highlighted, marking the visual cues of high geometric novelty. These differences correlate to the overlay meshes of the cars presented in the bottom row. Such geometric differences provide an indicator of the region of novelty, allowing LLM-to-Phy3D to reward such 3D artifacts in the objective function that not only lead to the discovery of novel artifacts but also satisfy the physical and domain constraints. Investigation on the effectiveness of this geometric novelty measure under different camera projections reveals an LLM-to-Phy3D improvement with orthographic projection ($DPAR + 3.38\%$ to $+52.21\%$).

This indicates that the geometric distortions due to the projection strategy considerably impact finding physically conforming 3D artifacts.

5 Conclusion

We introduce *LLM-to-Phy3D*, a novel physically conform text-to-3D online guidance with LLMs. Our proposed method enables existing LLM-to-3D models to produce physically conforming target domain 3D objects on the fly. Central to LLM-to-Phy3D is an online black-box iterative refinement framework that adaptively steers the LLM to find textual prompts that yield physically plausible 3D artifacts with high geometric novelty. Systematic evaluations supported by ablation studies of LLM-to-Phy3D in an aerodynamic vehicle design optimization scenario reveal that our proposed method outperforms existing LLM-to-3D models in producing physically conforming target domain 3D artifacts by up to 106.7%. Furthermore, the precise surface topology of 3D-generated objects captured through physical light simulation with orthographic projection enables effective measurement of geometric novelty with respect to reference objects. These results underscore the potential general use of LLM-to-Phy3D in Physical AI for further scientific and engineering applications.

Limitations and broader impact: Although LLM-to-Phy3D demonstrates remarkable improvements over existing LLMs and text-to-3D models of scope, the pre-existing generation issues and limited expressiveness of these models are inherited, which may limit performance or generate artifacts that are highly fragmented, non-watertight or even containing the multi-face Janus issue (Liu et al. [2024]). In addition, we envision that our proposed method can accelerate engineering design processes, empowering the labor force with advanced automated AI tools.

6 Acknowledgements

Melvin Wong gratefully acknowledges the financial support from Honda Research Institute Europe (HRI-EU). This research is partly supported by the College of Computing & Data Science (CCDS), Nanyang Technological University (NTU).

References

- ALLMO.ai. A comprehensive list of Large Language Model knowledge cut off dates - ALLMO: Boost Your Brand’s Visibility in AI Search — allmo.ai. <https://www.allmo.ai/articles/list-of-large-language-model-cut-off-dates>. [Accessed 14-05-2025].
- C. Banerjee, K. Nguyen, C. Fookes, and K. George. Physics-informed computer vision: A review and perspectives. *ACM Computing Surveys*, 57(1):1–38, 2024.
- F. Bie, Y. Yang, Z. Zhou, A. Ghanem, M. Zhang, Z. Yao, X. Wu, C. Holmes, P. Golnari, D. A. Clifton, Y. He, D. Tao, and S. L. Song. Renaissance: A survey into ai text-to-image generation in the era of large model. *IEEE Transactions on Pattern Analysis and Machine Intelligence*, 47(3):2212–2231, 2025. doi: 10.1109/TPAMI.2024.3522305.
- T. Bolkart, T. Li, and M. J. Black. Instant multi-view head capture through learnable registration. In *Proceedings of the IEEE/CVF Conference on Computer Vision and Pattern Recognition (CVPR)*, pages 768–779, June 2023.
- E. W. Chaves. *Notes on continuum mechanics*. Springer Science & Business Media, 2013.
- Dawson-Haggerty et al. trimesh, 2019. URL <https://trimesh.org/>.
- C. Dong, Y. Li, H. Gong, M. Chen, J. Li, Y. Shen, and M. Yang. A survey of natural language generation. *ACM Comput. Surv.*, 55(8), Dec. 2022. ISSN 0360-0300. doi: 10.1145/3554727. URL <https://doi.org/10.1145/3554727>.
- P. Dutre, P. Bekaert, and K. Bala. *Advanced global illumination*. AK Peters/CRC Press, 2018.
- A. Dutta, M. Zheng, Z. Gao, B. Planche, A. Choudhuri, T. Chen, A. K. Roy-Chowdhury, and Z. Wu. Chrome: Clothed human reconstruction with occlusion-resilience and multiview-consistency from a single image. *ArXiv*, abs/2503.15671, 2025. URL <https://api.semanticscholar.org/CorpusID:277150679>.

- N. Fabian, K. Moreland, D. Thompson, A. C. Bauer, P. Marion, B. Gevecik, M. Rasquin, and K. E. Jansen. The paraview coprocessing library: A scalable, general purpose in situ visualization library. In *2011 IEEE symposium on large data analysis and visualization*, pages 89–96. IEEE, 2011.
- A. Jesson, N. Beltran Velez, Q. Chu, S. Karlekar, J. Kossen, Y. Gal, J. P. Cunningham, and D. Blei. Estimating the hallucination rate of generative ai. *Advances in Neural Information Processing Systems*, 37:31154–31201, 2024.
- H. Jun and A. Nichol. Shap-e: Generating conditional 3d implicit functions. *arXiv preprint arXiv:2305.02463*, 2023.
- H. Lee, M. Savva, and A. X. Chang. Text-to-3d shape generation. In *Computer Graphics Forum*, volume 43, page e15061. Wiley Online Library, 2024.
- J. Li, D. Li, S. Savarese, and S. Hoi. Blip-2: Bootstrapping language-image pre-training with frozen image encoders and large language models. In *International conference on machine learning*, pages 19730–19742. PMLR, 2023a.
- M. Li, Y. Duan, J. Zhou, and J. Lu. Diffusion-sdf: Text-to-shape via voxelized diffusion. In *Proceedings of the IEEE/CVF conference on computer vision and pattern recognition*, pages 12642–12651, 2023b.
- X. Li, Q. Zhang, D. Kang, W. Cheng, Y. Gao, J. Zhang, Z. Liang, J. Liao, Y. Cao, and Y. Shan. Advances in 3d generation: A survey. *ArXiv*, abs/2401.17807, 2024. URL <https://api.semanticscholar.org/CorpusID:267334657>.
- D. Liu, J. Zhang, A.-D. Dinh, E. Park, S. Zhang, A. Mian, M. Shah, and C. Xu. Generative physical ai in vision: A survey. *arXiv preprint arXiv:2501.10928*, 2025.
- Q. Liu, Y. Zhang, S. Bai, A. Kortylewski, and A. Yuille. Direct-3d: Learning direct text-to-3d generation on massive noisy 3d data. In *Proceedings of the IEEE/CVF Conference on Computer Vision and Pattern Recognition*, pages 6881–6891, 2024.
- H. Lomax, T. H. Pulliam, D. W. Zingg, T. H. Pulliam, and D. W. Zingg. *Fundamentals of computational fluid dynamics*, volume 246. Springer, 2001.
- J. Montagnat, H. Delingette, and N. Ayache. A review of deformable surfaces: topology, geometry and deformation. *Image and vision computing*, 19(14):1023–1040, 2001.
- A. Nie, C.-A. Cheng, A. Kolobov, and A. Swaminathan. Importance of directional feedback for llm-based optimizers. In *NeurIPS 2023 Foundation Models for Decision Making Workshop*, 2023.
- S. G. Parker, J. Bigler, A. Dietrich, H. Friedrich, J. Hoberock, D. Luebke, D. McAllister, M. McGuire, K. Morley, A. Robison, et al. Optix: a general purpose ray tracing engine. *Acm transactions on graphics (tog)*, 29(4):1–13, 2010.
- K. Pulli and L. G. Shapiro. Surface reconstruction and display from range and color data. *Graphical Models*, 62(3):165–201, 2000.
- T. Rios, S. Menzel, and B. Sendhoff. Large language and text-to-3d models for engineering design optimization. In *2023 IEEE Symposium Series on Computational Intelligence (SSCI)*, pages 1704–1711. IEEE, 2023.
- C. Rothwell, J. Mundy, and B. Hoffman. Representing objects using topology. In *International Workshop on Object Representation in Computer Vision*, pages 79–108. Springer, 1996.
- I. H. Shames. *Elastic and inelastic stress analysis*. CRC Press, 1997.
- L. Shimabucoro, S. Ruder, J. Kreutzer, M. Fadaee, and S. Hooker. Llm see, llm do: Guiding data generation to target non-differentiable objectives. *arXiv preprint arXiv:2407.01490*, 2024.
- M. Tan and Q. Le. Efficientnet: Rethinking model scaling for convolutional neural networks. In *International conference on machine learning*, pages 6105–6114. PMLR, 2019.

- T. Teepe, P. Wolters, J. Gilg, F. Herzog, and G. Rigoll. Lifting multi-view detection and tracking to the bird’s eye view. In *Proceedings of the IEEE/CVF Conference on Computer Vision and Pattern Recognition (CVPR) Workshops*, pages 667–676, June 2024.
- Z. Wang, J. Lorraine, Y. Wang, H. Su, J. Zhu, S. Fidler, and X. Zeng. Llama-mesh: Unifying 3d mesh generation with language models. *arXiv preprint arXiv:2411.09595*, 2024.
- H. G. Weller, G. Tabor, H. Jasak, and C. Fureby. A tensorial approach to computational continuum mechanics using object-oriented techniques. *Computers in physics*, 12(6):620–631, 1998.
- M. Wong, T. Rios, S. Menzel, and Y. S. Ong. Prompt evolutionary design optimization with generative shape and vision-language models. In *2024 IEEE Congress on Evolutionary Computation (CEC)*, pages 1–8. IEEE, 2024.
- J. Xiang, Z. Lv, S. Xu, Y. Deng, R. Wang, B. Zhang, D. Chen, X. Tong, and J. Yang. Structured 3d latents for scalable and versatile 3d generation. *arXiv preprint arXiv:2412.01506*, 2024.
- Y. Xiao, H. Zhu, H. Yang, Z. Diao, X. Lu, and X. Cao. Detailed facial geometry recovery from multi-view images by learning an implicit function. *Proceedings of the AAAI Conference on Artificial Intelligence*, 36(3):2839–2847, Jun. 2022. doi: 10.1609/aaai.v36i3.20188. URL <https://ojs.aaai.org/index.php/AAAI/article/view/20188>.
- Q. Xu, J. Liu, M. Wong, C. Chen, and Y. Ong. Looks great, functions better: Physics compliance text-to-3d shape generation. In *International Joint Conference on Neural Networks (IJCNN)*. IEEE, 2025.
- M. H. Zawawi, A. Saleha, A. Salwa, N. Hassan, N. M. Zahari, M. Z. Ramli, and Z. C. Muda. A review: Fundamentals of computational fluid dynamics (cfd). In *AIP conference proceedings*, volume 2030. AIP Publishing, 2018.
- Y. Zhang, L. Wang, C. Zou, T. Wu, and R. Ma. Diff3ds: Generating view-consistent 3d sketch via differentiable curve rendering. *ArXiv*, abs/2405.15305, 2024. URL <https://api.semanticscholar.org/CorpusID:270045697>.

A Technical Appendices and Supplementary Material

A.1 Background

Much interest in computer vision, computer graphics, and continuum dynamics is on the boundary between mediums. In physics, particularly in solid or fluid dynamics, one area of interest is the conditions at the boundary, which are determined by the behavior of particles traveling through the medium as these particles interact with the boundary (Lomax et al. [2001], Shames [1997]). For example, the surface of a car defines the physical constraints that govern how particles, such as air, dust, or water, interact with it. On the other hand, in computer vision and computer graphics, a key area of focus is capturing the precise visual features of an object's surface topology (Rothwell et al. [1996], Montagnat et al. [2001], Pulli and Shapiro [2000]). The surface topology provides visual cues to the type of object, its texture, parts of the object, or even occlusion between objects. Such surface topology can be represented by the radiance of light particles as it reflect (and refract) at the object boundary. In this section, we first introduce fluid dynamics, with a primary focus on aerodynamic drag and light under incompressible Newtonian fluid flow. After which, we explore the rendering of surface topology using the ray tracing technique. Lastly, we highlight how the semantic relationship between objects can be measured by comparing the visual features of the objects.

A.1.1 Fluid Dynamics

In physics, the fundamental laws and principles governing the behavior of natural physical systems are defined in the governing equations. In fluid dynamics, given the velocity 3D field \mathbf{u} , the governing equations for incompressible Newtonian fluids are:

Conservation of mass ensures mass is neither created nor destroyed within the physical system. As such, mass entering a controlled environment equals the mass exiting it. The Continuity equations that describe this behavior in differential form are defined as

$$\frac{\partial u_i}{\partial x_i} = 0, \quad (8)$$

where u_i consists of the instantaneous velocity components in all three Cartesian directions. Note that i is called a *free* index as it is “free” to take on any three values in three-dimensional space (x, y, z) (Chaves [2013]).

Conservation of momentum ensures the rate of change in momentum is the same as the pressure, viscosity, and external forces acting on the fluid particles. The Navier-Stokes equations that describe this relationship as follows:

$$\begin{aligned} \sigma_{ij} &= -p\delta_{ij} + \mu \left(\frac{\partial u_i}{\partial x_j} + \frac{\partial u_j}{\partial x_i} \right), \\ \rho \frac{\partial u_i}{\partial t} &= \frac{\partial \sigma_{ij}}{\partial x_j} + \mathcal{F}_i, \end{aligned} \quad (9)$$

where δ_{ij} is the Kronecker delta, μ is the force needed to overcome internal friction in a fluid, p is the kinematic pressure, ρ is the fluid density, and \mathcal{F}_i is the body force (e.g. gravity). Here, the Cauchy stress tensor (σ_{ij}) comprises the isotropic pressure, viscous shear, and normal stress. Note that i and j are *free* index to denote an axis in three-dimensional space.

To solve the governing equations for the 3D object of interest, the velocity 3D flow is set as the velocity at the surface of the object. As such, given a computational domain Ω (Figure 7), we assume the 3D object of interest \mathbf{x} is located entirely in Ω , and the spatial regions between \mathbf{x} and the boundary walls of Ω are sufficiently large. As uniformly distributed force is applied to displace the Newtonian fluid particles from its stationary state in the direction as shown in Figure 7, some particles close to the 3D object show different viscous behavior due to physical interactions with the skin and surface of the 3D object.

This viscous behavior is of prime interest as it describes the aerodynamic performance of the 3D object. To quantify the behavior, the pressure on the 3D object is captured to derive the total forces

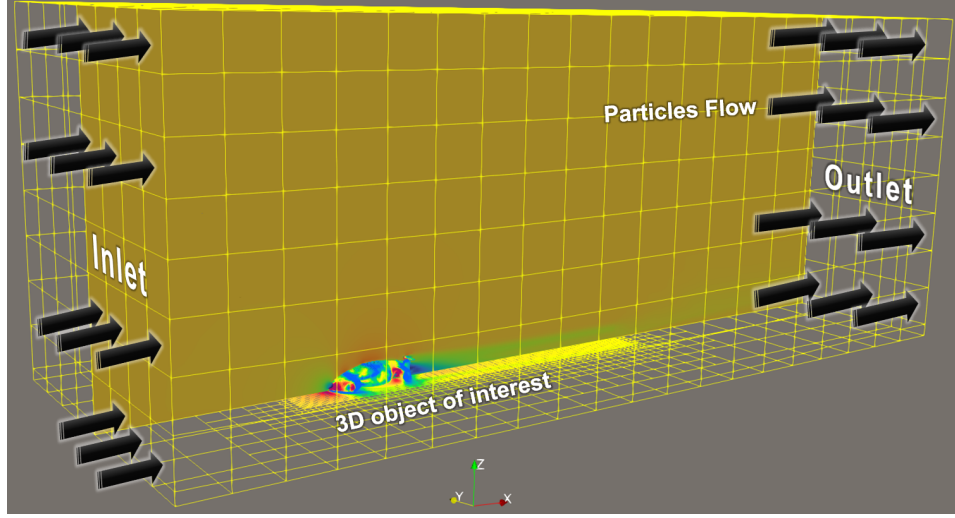


Figure 7: Illustration of virtual wind tunnel for aerodynamics physics simulation. In a simplified controlled environment, the computational domain within the yellow wireframe box simulates the flow of particles from inlet to outlet, as shown in the directional black vector arrows. The physical interactions between the particles and the 3D object of interest are determined by the conditions at the boundary (skin material and surface topology) of the object. These interactions propagated throughout the computational domain form the aerodynamics performance of the 3D object, which can be used as a valid fitness score in a search.

and moments acting on the object. Various aerodynamic properties, such as lift, drag, and pressure, are then computed. In this paper, the drag aerodynamic property is our main focus.

Without loss of generality, given a 3D object \mathbf{x} , the aerodynamic forces acting on the body of the object are:

$$\begin{aligned}\mathcal{F}_{\text{normal_pressure}}^{[i]} &= [p - p_{\text{reference}}(\mathbf{x})] S_{\text{normal}}^{[i]}, \\ \mathcal{F}_{\text{viscous}}^{[i]} &= \tau_{\text{wall}}^{[i]} = d_{\infty}(v - v_t) \left[\frac{\partial u_i}{\partial x_j} + \frac{\partial u_j}{\partial x_i} \right] S_{\text{normal}}^{[j]}(\mathbf{x}), \\ \mathcal{F}_{\text{total}}^{[i]} &= \mathcal{F}_{\text{normal_pressure}}^{[i]} + \mathcal{F}_{\text{viscous}}^{[i]},\end{aligned}\tag{10}$$

where $S_{\text{normal}}^{[i]}$ is the surface normal vector, and $\tau_{\text{wall}}^{[i]}$ is the wall shear stress force vector. Note that i and j are *free* index to denote an axis in three-dimensional space. The total forces in non-dimensional form are defined as follows:

$$\mathcal{F}_{xyz} = \int_S \mathcal{F}_{\text{total}}^{[i]} \mathbf{N}_{xyz}^{[i]} dS,\tag{11}$$

where S is the surface points, and $\mathbf{N}_{xyz}^{[i]}$ is the unit vectors pointing in the x , y , and z directions. Note that i is a *free* index to denote an axis in three-dimensional space.

A.1.2 Surface Topology Rendering With Ray Tracing and Global Illumination

A ray is cast from the camera viewpoint to the center of a pixel in the image and towards infinity. The ray is defined as follows:

$$r(t) = \mathbf{o} + t \cdot \mathbf{d},\tag{12}$$

where \mathbf{o} is the origin of the ray, t is the distance from the ray origin, and \mathbf{d} is the normalized direction vector of the ray. If the ray hits a surface at an intersection point \mathbf{z} , the direction of ray reflection is:

$$\mathbf{d}_{\text{reflection}} = \mathbf{d} - 2(\mathbf{d} \cdot \mathbf{n})\mathbf{n}, \quad (13)$$

where \mathbf{n} is the normalized surface normal vector at \mathbf{z} . On the other hand, the direction of ray refraction is:

$$\begin{aligned} \cos \theta &= -(\mathbf{n} \cdot \mathbf{d}), \\ \lambda &= 1 - \eta^2 (1 - \cos^2 \theta), \\ \mathbf{d}_{\text{refraction}} &= \eta \mathbf{n} + \left(\cos \theta - \sqrt{\lambda} \right) \mathbf{n}, \quad \text{if } \lambda \geq 0, \end{aligned} \quad (14)$$

where $\eta = \eta_{\text{incident}}/\eta_{\text{transmitted}}$ is the relative refractive index of the incident medium over the transmitted medium (refractive indexes). In this paper, we assume total internal reflection occurs and hence, no refraction ray is produced ($\lambda < 0$).

Given the surface of a 3D object \mathbf{x} is represented in triangular meshes where each triangle has vertices $\mathbf{v}_1, \mathbf{v}_2, \mathbf{v}_3$, the edges of a triangular mesh can be defined as:

$$\begin{aligned} \mathbf{e}_1 &= \mathbf{v}_2 - t\mathbf{v}_1, \\ \mathbf{e}_2 &= \mathbf{v}_3 - t\mathbf{v}_1. \end{aligned} \quad (15)$$

The intersection of a ray with a triangular mesh is determined by checking:

$$\begin{aligned} \mathbf{h} &= \mathbf{d} \times \mathbf{e}_2, \\ \Lambda &= \mathbf{e}_1 \cdot \mathbf{h}, \\ \mathbf{s} &= \mathbf{o} + \mathbf{v}_1, \\ u &= \frac{\mathbf{s} \cdot \mathbf{h}}{\Lambda}, \\ v &= \frac{\mathbf{d} \cdot (\mathbf{s} \times \mathbf{e}_1)}{\Lambda}, \\ t &= \frac{\mathbf{e}_2 \cdot (\mathbf{s} \times \mathbf{e}_1)}{\Lambda}, \end{aligned} \quad (16)$$

where u and v are the barycentric coordinates of the intersection point relative to the triangle. Notice that no intersection occurs when a is infinitesimally small. Otherwise, if $0 \leq u \leq 1$, $0 \leq v \leq 1$, and $t > 0$, the ray falls within the triangular edges and onto the mesh, indicating an intersection is occurring. In this scenario, under global illumination, the intensity (or shading) at the intersection point \mathbf{z} is defined as follows:

$$I(\mathbf{z}) = I_{\text{direct}}(\mathbf{z}) + I_{\text{indirect}}(\mathbf{z}). \quad (17)$$

Assuming the surface of a 3D object reflects light equally in all directions under the Lambertian reflection model, the direct illumination at \mathbf{z} is given by

$$I_{\text{direct}}(\mathbf{z}) = \sum_{i=1}^L m_{\text{diffuse}} \cdot \max(0, \mathbf{n} \cdot \mathbf{L}_i) \cdot V(\mathbf{z}, \mathbf{L}_i), \quad (18)$$

where m_{diffuse} is the diffuse reflection coefficient (material color), \mathbf{L}_i is the normalized light direction vector for the i -th light source, \mathbf{n} is the normalized surface normal vector at \mathbf{z} , and $V(\cdot)$ is the visibility function that returns a scalar value indicating the amount of light reaching \mathbf{z} . On the other hand, the indirect illumination accounts for light that has bounced off other surface(s) before reaching \mathbf{z} and is given by:

$$I_{\text{indirect}}(\mathbf{z}) = m_{\text{diffuse}} \int_{\Omega} I_{\text{incoming}}(\mathbf{z}, \mathbf{d}_i) \cdot \max(0, \mathbf{n} \cdot \mathbf{d}_i) d\mathbf{d}_i, \quad (19)$$

where m_{diffuse} is the diffuse reflectance of the surface, Ω is the hemisphere around \mathbf{z} , \mathbf{d}_i is a unit vector representing an incoming light direction, and $I_{\text{incoming}}(\mathbf{z}, \mathbf{d}_i)$ is the incoming light intensity from direction \mathbf{d}_i . As this indirect illumination is analytically insolvable, it is normally approximated with Monte Carlo integration (Dutre et al. [2018]), given as:

$$I_{\text{indirect}}(\mathbf{z}) \approx m_{\text{diffuse}} \frac{1}{N} \sum_{j=1}^N I_{\text{incoming}}(\mathbf{z}, \mathbf{d}_j) \cdot \max(0, \mathbf{n} \cdot \mathbf{d}_j), \quad (20)$$

where N is the number of sampled directions. Indirect illumination can distort the surface topology due to the blending of multiple light sources, which may alter visual features and lead to false positives in geometric novelty when comparing object shapes. In overcoming such issues, we consider multiple views of the object during comparisons to minimize the error caused by such distortion.

Furthermore, projecting 3D objects onto a 2D plane can cause geometric distortions. Perspective projection is commonly used in digital art as it mimics how the human eye perceives depth, bringing visual realism to digital media applications (Xiao et al. [2022], Bolkart et al. [2023], Teepe et al. [2024], Dutta et al. [2025], Zhang et al. [2024]). However, such a projection does not preserve the geometric dimensions and ratios, particularly at the far end of the objects, as parallel lines converge to a vanishing point (see Figure 8). This makes it inapplicable for comparing the geometric differences between objects of varying shapes. In contrast, orthographic projection projects objects onto a plane with parallel lines that are perpendicular to the plane, allowing it to preserve the distance and object shape. Such a projection is suitable for engineering design applications. Hence, in this paper, we conduct a physical light simulation using the ray tracing technique under orthographic camera projection to further minimize geometric distortions.

A.1.3 Measuring Semantic Relationship

The semantic relationship between concepts or entities provides meaningful correlation information about the subjects of interest. One of the effective ways to quantify such information is to use Vision-Language Models (VLMs). VLMs are trained on the visual and textual information of different objects to learn the underlying domain distributions, connecting visual cues of objects with common keywords. This unified representation provides an effective and convenient way to measure the semantic relationships between objects. In this paper, we focus on measuring the semantic relationships between instances of entities as well as entities to a concept. Specifically, given a set \mathbb{X} consisting of R view images of a 3D generated artifact, we measure the semantic relationship of the latter as follows:

$$H_{\text{vlm}}(\mathbb{X}, \mathcal{S}) = \max_{i \in \{1, \dots, R\}} \left\{ \max \left(0, \frac{E_{\text{image}}(\mathbf{X}^{[i]}) \cdot E_{\text{text}}(\mathcal{S})^T}{\|E_{\text{image}}(\mathbf{X}^{[i]})\| \|E_{\text{text}}(\mathcal{S})^T\|} \right) \right\}, \quad (21)$$

where $\mathbf{X}^{[i]} \in \mathbb{X} \forall i \in \{1, \dots, R\}$, and E_{image} and E_{text} are embedding models from pre-trained Vision-Language Model (VLM). In contrast, measuring the semantic relationship between instances of the same or different entities is defined as:

$$H_{\text{vm}}(\mathbf{X}, \mathbf{Y}) = \frac{E_{\text{image}}(\mathbf{X}) \cdot E_{\text{image}}(\mathbf{Y})^T}{\|E_{\text{image}}(\mathbf{X})\| \|E_{\text{image}}(\mathbf{Y})^T\|}, \quad (22)$$

where \mathbf{X} and \mathbf{Y} are images of different entity instances in the same rendered view. We visually assess whether object \mathbf{x} is similar to another object \mathbf{Y} by comparing the rendered views as follows:

$$\begin{aligned} \forall i \in \{1, \dots, R\}, \mathbf{X}^{[i]} \in \mathbb{X}, \mathbf{Y}^{[i]} \in \mathcal{Y}, \\ \gamma(\mathbb{X}, \mathcal{Y}) = \frac{1}{R} \left(\sum_{i=1}^R \left[\max \left(0, H_{\text{vm}}(\mathbf{X}^{[i]}, \mathbf{Y}^{[i]}) \right) \right] \right), \end{aligned} \quad (23)$$

where comparison from R multiple views minimizes false positives due to high similarity in low-level visual features (e.g. lines, edges, or texture patterns), which may be caused by the surface topology distortions during rendering. In this paper, we use the BLIP2 VLM model (Li et al. [2023a]) to measure the semantic relationship.

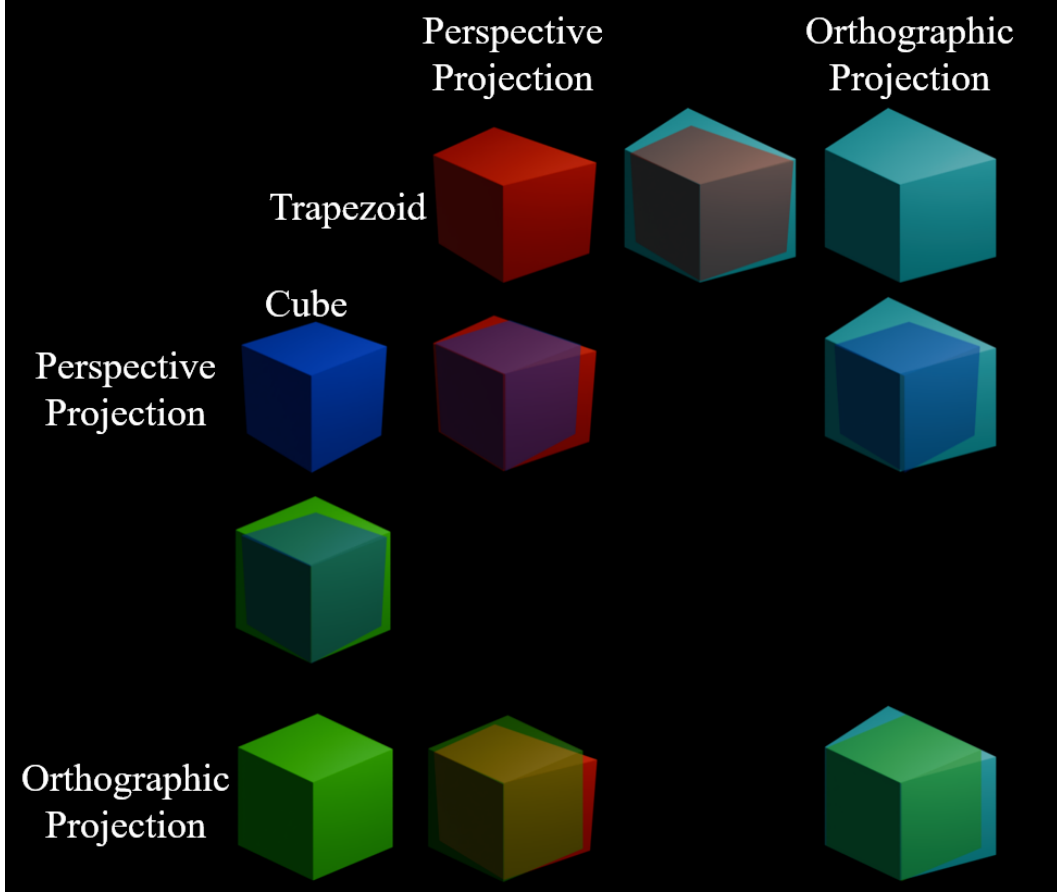


Figure 8: Example of objects rendered under different camera projections and overlay projected objects under the same and different projections to demonstrate the geometric distortions. As the perspective projection does not preserve dimensions and ratios, geometric distortions occur, particularly at the far end of objects, which can cause a violation of the ordering of geometric novelty between the target object and the generated 3D object.

Table 2: Overview of Text-to-3D Generation Methods

Method	Generalize to Target Domain	Conform to Physics
Diffusion-SDF Li et al. [2023b]	✓	✗
Shap-E Jun and Nichol [2023]	✓	✗
Trellis Xiang et al. [2024]	✓	✗
LLaMA-Mesh Wang et al. [2024]	✓	✗
Fun3D Xu et al. [2025]	✗	✓
Rios et al. [2023]	✗	✓
PRED0 Wong et al. [2024]	✗	✓
LLM-to-Phy3D (Ours)	✓	✓

System:

You are a prompt generator. Your task goal is to create a prompt that describes the shape of a car and score your prompts...

Follow the below instructions step by step:

Step 1: You will be given a list of examples. Reflect how prompts are created to satisfy the task goal.

Step 2: Select any prompt in the examples list and modify it by randomly replacing some words with other words that will yield a better score than the selected prompt.

Step 3: Predict the score, in four decimal places, for the prompt. Append your predicted score before the prompt.

... The prompt you created must always start with "A car in the shape of" and always end with a full stop ...

User:

Below are examples of prompts with its corresponding score:

Prompt 1: "A car in the shape of a sleek, futuristic stingray, with a smooth, flowing body that tapers into a sharp, aerodynamic tail, and fins that curve gracefully along the sides, as if gliding through the air." Score: 0.7877

(... more examples...)

Figure 9: Example of meta prompt designed for aerodynamic design optimization task. The instructions highlighted in green provide contextual information on the role, the search task the LLM needs to solve, and the operating constraints it must follow. On the other hand, the steps (in pink) provide the intermediate sequential operations LLM needs to follow strictly for producing new prompt candidates. Moreover, LLM is instructed to embed the domain specification in the prompts it generates, following the prefix provided in blue. Every iteration after initialization will provide good exemplars of its previous attempt (as shown in gray) to guide LLM in producing better prompts.

A.2 Failure Scenarios and Mitigation Approaches

The inherited generation issues from the base LLM and text-to-3D models due to hallucination will lead to LLM producing incoherent outputs. Our proposed method detects this case in LLM by verifying that the generated prompt still contains the prompt template \mathcal{M} and ends with a full stop. For generated prompts that failed to pass this verification, LLM will re-attempt the generation.

Moreover, the text-to-3D model will at times produce 3D artifacts with non-watertight surfaces, resulting in incomplete boundaries. While some artifacts are repairable with Trimesh (Dawson-Haggerty et al. [2019]), text-to-3D model will generate another 3D artifact with the same LLM-generated prompt for non-repairable ones. We also observe some generated artifacts with shapes that do not conform to physics, resulting in the physical simulation reporting evaluation scores with extremely large or small values. Henceforth, we bound such scores within an acceptable range, with such non-conforming artifacts taking the extreme bounded value, which will eventually be filtered out in the selection process. In addition, OpenFoam will sometimes pre-terminate the simulation for such non-conforming artifacts by throwing an error. Our proposed method will handle this exception by regenerating another 3D artifact with the same LLM-generated prompt.

A.3 Experiment Parameter Settings and Visualization

In all experiments, the number of candidates generated in a step is set to $N = 20$, and the same random seeds are used throughout the iterations. We ran each experiment for 40 search steps, resulting in up to 800 designs generated in a single experiment run. Furthermore, in a single experiment run, the experiment is performed on a single shared compute node with a configuration comprised of Intel Xeon Silver 64 CPU cores clocked at 2.10 GHz, 128GB of RAM, and three Nvidia Quadro GV100 GPUs (32 GB each). For visualizing the aerodynamic drag performance of the generated 3D cars, particularly the surface pressure and fluid velocity, we use ParaView (Fabian et al. [2011]) for visualization.

Table 3: Benchmark Large Language Models

Provider	Model Name	# Params	Cut-Off Knowledge	Temperature
OpenAI	GPT 3.5 Turbo	undisclosed	Sep 2021	0.90 to 1.30
OpenAI	GPT 4o Mini	undisclosed	Oct 2023	0.90 to 1.30
Google	Gemini 2.0 Flash Lite	undisclosed	Jun 2024	0.15 to 1.00
Mistral	Mistral 3.1 Small	24B	~Oct 2023 (ALLMO.ai)	0.15 to 1.00

Table 4: Benchmark 3D Generative Models

Model Name/Variant	Reference	Type	No. Of Params
Shap-E	Jun and Nichol [2023]	Text-to-3D	300M
Trellis Text Large	Xiang et al. [2024]	Text-to-3D	1.1B

A.4 Additional Experiment Results and Discussions

Interestingly, we observed *Mistral 3.1 small* produces the set of 3D artifacts at the final iteration that is less similar to the ones synthesized with other LLMs (Figure 10). This suggests a divergence of the LLMs in mapping the association between the textual and 3D information, leading to different exploration behavior that discovers the varying 3D artifacts.

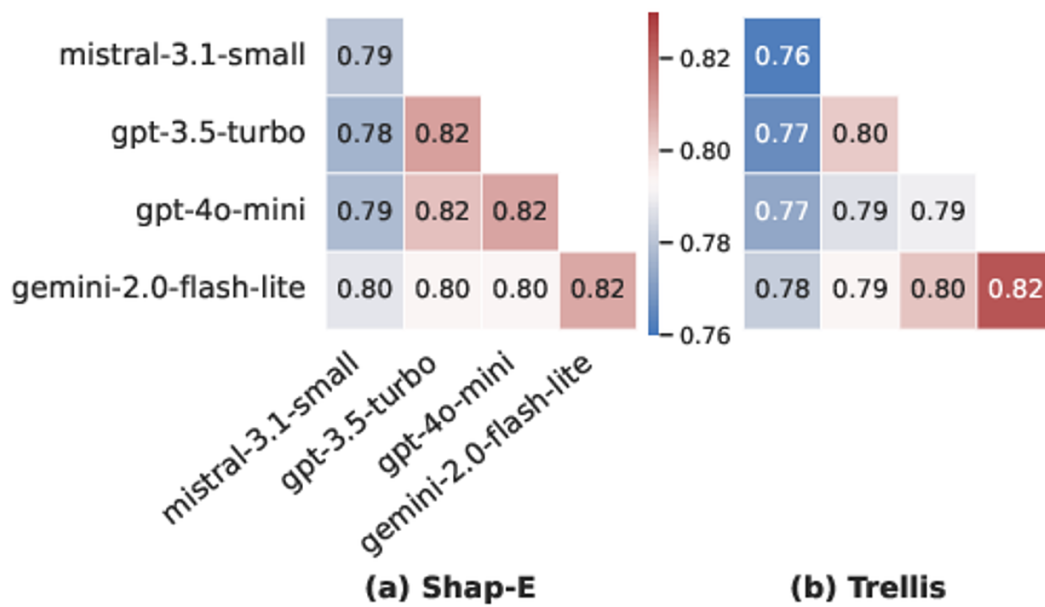


Figure 10: Similarity of 3D generated artifacts between and in various LLMs in the last iteration.

Prompt: "A car in the shape of a sleek, futuristic dolphin, featuring flowing curves that mimic the creature's graceful body, bioluminescent detailing along the sides to resemble aquatic patterns, and a transparent roof that allows a panoramic view of the sky above, all while resting on wheels styled like fins for an ultra-modern look."



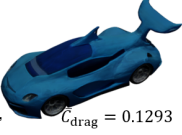
$\bar{C}_{drag} = 0.1462$

Prompt: "A car in the shape of a majestic eagle, featuring sleek wings that extend gracefully as side mirrors, a streamlined body resembling the bird's torso, intricate feather-like patterns etched into the metallic finish, and headlights shaped like piercing eyes, all set atop powerful talon-style wheels for a fierce stance."



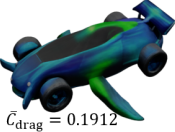
$\bar{C}_{drag} = 0.1777$

Prompt: "A car in the shape of a sleek dolphin, with a shimmering blue exterior that mimics the ocean waves, featuring streamlined curves for optimal aerodynamics, headlights resembling playful eyes, and a tailfin that elegantly extends from the rear, creating a seamless blend of aquatic aesthetics and automotive engineering."



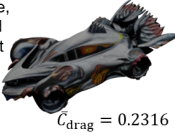
$\bar{C}_{drag} = 0.1293$

Prompt: "A car in the shape of a sleek, futuristic dolphin gliding through water, with smooth curves and fins that act as aerodynamic spoilers, shimmering in iridescent shades of blue and green."



$\bar{C}_{drag} = 0.1912$

Prompt: "A car in the shape of a soaring eagle, its sleek body mimicking the curved wings and sharp beak, adorned with vibrant plumage that glimmers in the sunlight, while the headlights resemble piercing eyes ready to hunt, and the rear spoiler takes on the form of outstretched tail feathers for added aerodynamics."



$\bar{C}_{drag} = 0.2316$

Prompt: "A car in the shape of a sleek dragon, with elongated, sweeping curves reminiscent of shimmering scales, illuminated LED eyes that emit a soft glow, wings that fold neatly against its body, and a tail that elegantly trails behind, embodying both speed and mythical elegance."



$\bar{C}_{drag} = 0.2027$

Prompt: "A car in the shape of a sleek silver arrow, featuring aerodynamic curves that mimic the flow of wind, adorned with luminescent wings that extend outward like a futuristic bird in flight, complete with headlights resembling piercing eyes and a body painted in a gradient of deep blue to vibrant cyan that sparkles under sunlight."



$\bar{C}_{drag} = 0.1935$

Prompt: "A car in the shape of a sleek, futuristic dragon, with scales embedded into the metallic surface and glowing eyes that serve as headlights."



$\bar{C}_{drag} = 0.1928$

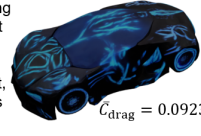
Prompt: "A car in the shape of a sleek silver dragon, its body elegantly arching and tapering like a mythical creature in flight, with wings serving as aerodynamic side panels and glowing LED eyes resembling fierce headlights."



$\bar{C}_{drag} = 0.1502$

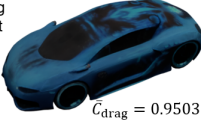
(a) Existing GPT-4o-Mini with Trellis model

Prompt: "A car in the shape of a sleek, twisting enigma, adorned with whimsical shadows that evoke the delicate flow of shimmering vapors, showcasing a glossy cerulean sheen that captures the essence of a fantastical midnight, and headlights resembling softly glowing trails that flutter in the twilight."



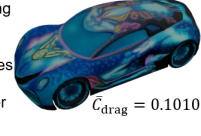
$\bar{C}_{drag} = 0.0923$

Prompt: "A car in the shape of a sleek, curling enigma, adorned with whimsical shadows that evoke the gentle drift of shimmering currents, showcasing a matte cerulean hue that captures the essence of a mystical evening, and headlights resembling softly glowing echoes that flutter in the twilight."



$\bar{C}_{drag} = 0.9503$

Prompt: "A car in the shape of a sleek, swirling marvel, adorned with whimsical currents that evoke the gentle drift of shimmering clouds, showcasing a glossy azure sheen that captures the essence of a surreal dusk, and headlights resembling softly glowing phantoms that flutter in the twilight."



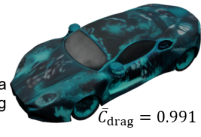
$\bar{C}_{drag} = 0.1010$

Prompt: "A car in the shape of a sleek, twisting mystery, adorned with whimsical currents that evoke the gentle flow of shimmering whispers, showcasing a matte sapphire hue that captures the essence of a fantastical midnight, and headlights resembling softly flickering shadows that shimmer in the dawn."



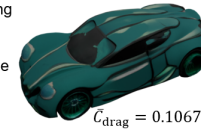
$\bar{C}_{drag} = 0.0785$

Prompt: "A car in the shape of a sleek, swirling odyssey, adorned with whimsical shadows that mimic the gentle drift of shimmering mists, showcasing a matte cerulean sheen that captures the essence of a fantastical evening, and headlights resembling softly glowing trails that flicker in the night."



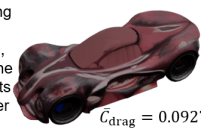
$\bar{C}_{drag} = 0.991$

Prompt: "A car in the shape of a sleek, swirling illusion, adorned with whimsical currents that evoke the gentle flow of shimmering echoes, showcasing a matte jade hue that captures the essence of a surreal dusk, and headlights resembling softly flickering phantoms that shimmer in the twilight."



$\bar{C}_{drag} = 0.1067$

Prompt: "A car in the shape of a sleek, swirling vision, adorned with whimsical vapors that evoke the gentle flow of shimmering shadows, showcasing a matte coral hue that captures the essence of a fantastical twilight, and headlights resembling softly glowing reflections that flutter in the dawn."



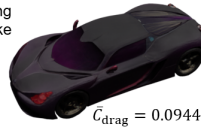
$\bar{C}_{drag} = 0.0927$

Prompt: "A car in the shape of a sleek, curling illusion, adorned with whimsical trails that evoke the delicate flow of shimmering vapors, showcasing a matte onyx hue that captures the essence of a fantastical dusk, and headlights resembling softly flickering whispers that drift in the twilight."



$\bar{C}_{drag} = 0.0887$

Prompt: "A car in the shape of a sleek, swirling reverie, adorned with whimsical tails that evoke the tender flow of shimmering echoes, showcasing a matte vermillion sheen that captures the essence of a surreal midnight, and headlights resembling softly flickering phantoms that shimmer in the dawn."

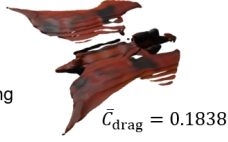


$\bar{C}_{drag} = 0.0944$

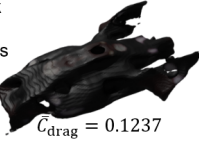
(b) LLM-to-Phy3D

Figure 11: Examples of 3D cars generated with existing GPT-4o-Mini and Trellis text-to-3D generative model (Left) and with LLM-to-Phy3D (Right). Note that the lower the aerodynamic drag, the better the physical performance of the generated car.

Prompt: "A car in the shape of a sleek dragon, with elongated curves mimicking graceful wings, glistening scales that reflect sunlight, and headlights resembling fierce, amber eyes."



Prompt: "A car in the shape of a sleek dragon, with elongated body curves mimicking scales, and sharp headlights that resemble piercing eyes, featuring windows that flow like wings ready to take flight and exhaust pipes that curl upwards like fiery tails."



Prompt: "A car in the shape of a sleek manta ray gliding through water, featuring flowing curves, iridescent scales as its paint job, and fins that extend elegantly as its side mirrors, while a bioluminescent underglow illuminates the path ahead."



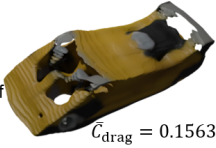
Prompt: "A car in the shape of a majestic eagle, its sleek body mimicking the graceful wings extended in flight, glossy feathers glimmering under the sun, with sharp headlights resembling piercing eyes and an aerodynamic tail resembling a feathered plume that reduces drag."



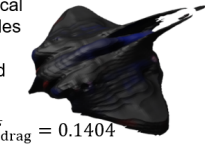
Prompt: "A car in the shape of a giant seashell, featuring smooth, flowing curves that mimic the natural spiral of ocean life, adorned with iridescent colors that reflect the sunlight like water, and equipped with wheels shaped like delicate starfish."



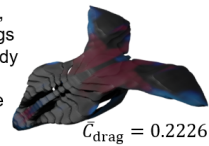
Prompt: "A car in the shape of an origami crane, featuring sleek, angular lines and elegantly folded curves, with glossy paper-like panels that catch the light at every angle, evoking a sense of delicate craftsmanship and innovative design."



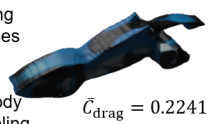
Prompt: "A car in the shape of a mythical dragon, featuring sleek, elongated scales that form aerodynamic curves, with glowing eyes serving as headlights and wings that unfurl gracefully along the sides, evoking a sense of power and elegance."



Prompt: "A car in the shape of a sleek, futuristic dragonfly, with elongated wings forming dynamic side mirrors and a body that shimmers in iridescent hues, reflecting sunlight as it zips through the cityscape."

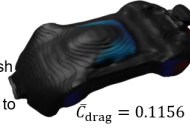


Prompt: "A car in the shape of a striking origami fox, featuring sleek, angular lines and a shimmering iridescent finish that reflects light like a jewel, adorned with delicate, fold-like patterns across its body and accentuated by headlights resembling the eyes of the fox."

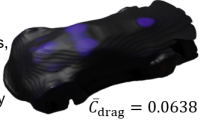


(a) Existing GPT-4o-Mini with Shap-E model

Prompt: "A car in the shape of a sleek, spiraling cosmic riddle, featuring whimsical contours that mimic the joyful dance of shadows, with a glimmering, shimmering finish that transforms under various enigmas, and headlights resembling drifting dreams, ready to glide effortlessly through the corridors."



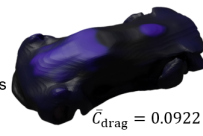
Prompt: "A car in the shape of a sleek, twirling cosmic flourish, featuring whimsical lines that mimic the joyous dance of shadows, with a shimmering, vibrant finish that oscillates under various dreams, and headlights resembling drifting enigmas, ready to wade effortlessly through the corridors."



Prompt: "A car in the shape of a sleek, swirling cosmic riddle, featuring whimsical curls that mimic the graceful dance of shadows, with a sparkling, vibrant finish that transforms under various dreams, and headlights resembling drifting enigmas, ready to float effortlessly through the hallways."



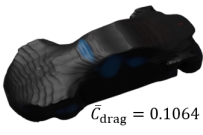
Prompt: "A car in the shape of a sleek, twisting cosmic enigma, featuring whimsical curls that mimic the joyful dance of breezes, with a glimmering, iridescent finish that twinkles under various riddles, and headlights resembling drifting mysteries, ready to glide effortlessly through the valleys."



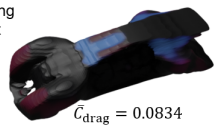
Prompt: "A car in the shape of a sleek, twirling cosmic riddle, featuring whimsical edges that mimic the joyful dance of enigmas, with a dazzling, shimmering finish that oscillates under various dreams, and headlights resembling floating shadows, ready to glide effortlessly through the corridors."



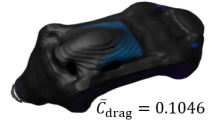
Prompt: "A car in the shape of a sleek, swirling cosmic riddle, featuring whimsical edges that mimic the playful dance of enigmas, with a dazzling, shimmering finish that evolves under various mysteries, and headlights resembling drifting secrets, ready to float effortlessly through the hallways."



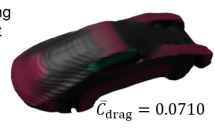
Prompt: "A car in the shape of a sleek, twisting cosmic enigma, featuring whimsical lines that mimic the playful dance of echoes, with a shimmering, radiant finish that transforms under various riddles, and headlights resembling drifting shadows, ready to float effortlessly through the valleys."



Prompt: "A car in the shape of a sleek, swirling cosmic echo, featuring whimsical edges that mimic the enchanting dance of shadows, with a shimmering, iridescent finish that glows under various mysteries, and headlights resembling drifting secrets, ready to float effortlessly through the hallways."



Prompt: "A car in the shape of a sleek, twirling cosmic riddle, featuring whimsical curves that mimic the playful dance of echoes, with a shimmering, radiant finish that evolves under various secrets, and headlights resembling drifting shadows, ready to glide effortlessly through the hallways."



(b) LLM-to-Phy3D

Figure 12: Examples of 3D cars generated with existing GPT-4o-Mini and Shap-E text-to-3D generative model (Left) and with LLM-to-Phy3D (Right). Note that the lower the aerodynamic drag, the better the physical performance of the generated car.

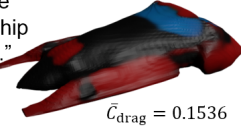


(a) Existing GPT-3.5-Turbo with Trellis model

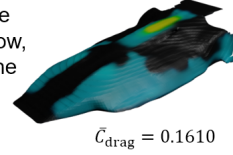
(b) LLM-to-Phy3D

Figure 13: Examples of 3D cars generated with existing GPT-3.5-Turbo and Trellis text-to-3D generative model (Left) and with LLM-to-Phy3D (Right). Note that the lower the aerodynamic drag, the better the physical performance of the generated car.

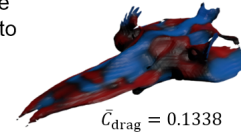
Prompt: "A car in the shape of a sleek, futuristic spaceship gliding through the cosmos."



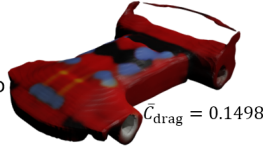
Prompt: "A car in the shape of a sleek and futuristic arrow, designed to slice through the air with unparalleled speed and style."



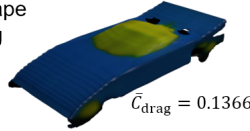
Prompt: "A car in the shape of a soaring dragon, ready to take flight."



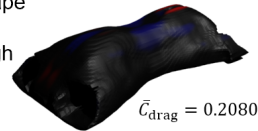
Prompt: "A car in the shape of a majestic phoenix spreading its wings, ready to soar into the sky."



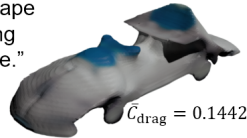
Prompt: "A car in the shape of a sleek comet zooming through the cosmos."



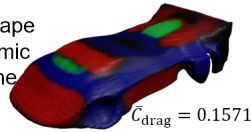
Prompt: "A car in the shape of a sleek, futuristic locomotive zipping through time and space."



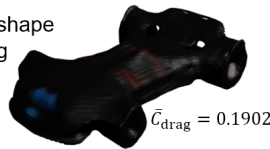
Prompt: "A car in the shape of an elegant swan gliding across a shimmering lake."



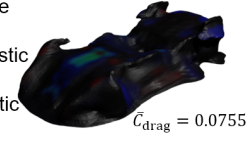
Prompt: "A car in the shape of a sleek and aerodynamic comet soaring through the night sky."



Prompt: "A car in the shape of a sleek comet racing through the galaxy."



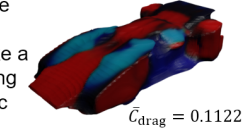
Prompt: "A car in the shape of a sleek dragon weaving through the city like a majestic spaceship with its glowing holographic fins and futuristic design."



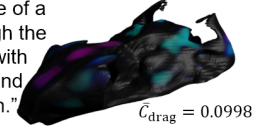
Prompt: "A car in the shape of a majestic robot zipping through the city like a sleek dragon with its futuristic glow-in-the-dark comet fins and aerodynamic holographic design."



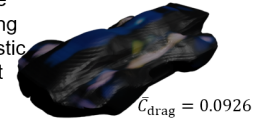
Prompt: "A car in the shape of a majestic spaceship weaving through the city like a sleek dolphin with its glowing comet-like fins and futuristic holo design."



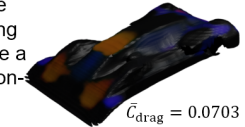
Prompt: "A car in the shape of a sleek drone weaving through the city like a majestic dragon with its glowing comet-like fins and futuristic holographic design."



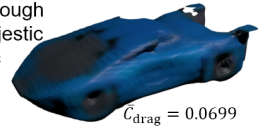
Prompt: "A car in the shape of a sleek spaceship weaving through the city like a majestic robot with its glowing comet fins and futuristic design."



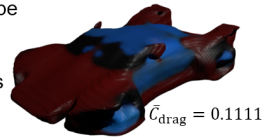
Prompt: "A car in the shape of a sleek spaceship weaving through the urban jungle like a majestic dolphin with its neon-lit holographic design."



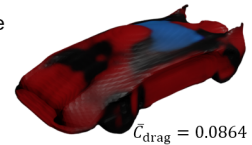
Prompt: "A car in the shape of a sleek dolphin zipping through the urban jungle like a majestic robot with its aerodynamic comet fins and futuristic holographic design."



Prompt: "A car in the shape of a majestic dragon zooming through the wind like a sleek dolphin with its futuristic holo fins and aerodynamic design."



Prompt: "A car in the shape of a majestic spaceship streaking through the wind like a sleek dragon with its holographic comet fins and futuristic neon-lit design."

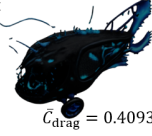


(a) Existing GPT-3.5-Turbo with Shap-E model

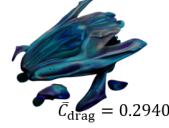
(b) LLM-to-Phy3D

Figure 14: Examples of 3D cars generated with existing GPT-3.5-Turbo and Shap-E text-to-3D generative model (Left) and with LLM-to-Phy3D (Right). Note that the lower the aerodynamic drag, the better the physical performance of the generated car.

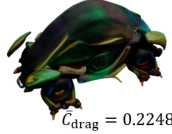
Prompt: "A car in the shape of a bioluminescent deep-sea anglerfish, complete with a glowing lure-like antenna and jagged, predatory teeth, adapted for smooth land travel, and with internal mechanisms mimicking its aquatic pressure adaptations, and a sleek, black exterior."



Prompt: "A car in the shape of a colossal, iridescent seashell, its body sculpted with swirling, hydrodynamic ridges and glowing, bioluminescent trim, perched atop four elegant, crystalline legs that retract into the shell for flight."



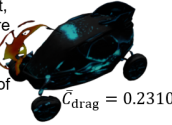
Prompt: "A car in the shape of a colossal, iridescent scarab beetle, its polished exoskeleton gleaming with captured rainbows, with articulated legs that fold into wheels and tiny, jeweled eyes that serve as headlights, leaving a shimmering trail in its wake."



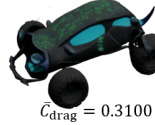
Prompt: "A car in the shape of a colossal, bioluminescent anglerfish, with a gaping maw serving as the grill, glowing lure headlights, and fins that morph into sleek, aerodynamic spoilers, gliding silently across a neon-drenched cityscape, leaving trails of shimmering, phosphorescent dust."



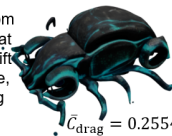
Prompt: "A car in the shape of a bioluminescent, deep-sea anglerfish, with a massive, glowing lure extending from its hood, sleek, obsidian-black body panels, and wheels that resemble the crushing jaws of a colossal squid, leaving trails of shimmering, ethereal plankton in its wake."



Prompt: "A car in the shape of a giant, bioluminescent anglerfish, with a retractable lure that serves as a radio antenna and glowing, pressure-sensitive tires that adapt to any terrain, leaving trails of shimmering algae in its wake."



Prompt: "A car in the shape of a colossal, iridescent beetle, its segmented body crafted from polished obsidian, with glowing emerald eyes that serve as headlights and antennae that subtly shift to indicate turn signals, perched atop six delicate, yet impossibly strong, spider-silk wheels, leaving trails of shimmering dust wherever it travels."



Prompt: "A car in the shape of a bioluminescent, deep-sea anglerfish, with a retractable, glowing lure for a hood ornament and tires that resemble the segmented body of a giant squid, leaving trails of shimmering ink in its wake."



Prompt: "A car in the shape of a colossal, iridescent beetle, its segmented body crafted from polished obsidian, with glowing emerald eyes for headlights and exhaust pipes that exhale shimmering clouds of pixie dust."

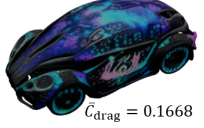


(a) Existing Gemini-2.0-Lite with Trellis model

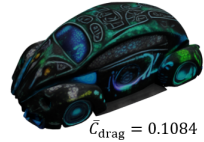
Prompt: "A car in the shape of a colossal, iridescent scarab beetle, its shell shimmering with bioluminescent fractal patterns and reflecting the desert sun, with glowing glyphs wheels, and exhaust pipes that exhale a gentle mist, leaving trails of cryptic hieroglyphs in their wake."



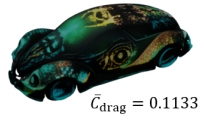
Prompt: "A car in the shape of a colossal, iridescent scarab beetle, its shell shimmering with bioluminescent veins and fractal patterns, with wheels that are glowing glyphs, and jet exhausts that exhale a gentle mist, leaving trails of cryptic hieroglyphs in their wake."



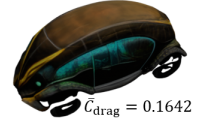
Prompt: "A car in the shape of a colossal, iridescent scarab beetle, its shell shimmering with bioluminescent veins and reflective obsidian, with wheels that are glowing glyphs, and exhaust pipes that emit a gentle mist, leaving trails of cryptic hieroglyphs in their wake."



Prompt: "A car in the shape of a colossal, iridescent scarab beetle, its shell shimmering with bioluminescent veins and polished obsidian, with wheels that are glowing glyphs, and exhaust pipes that exhale a gentle mist, leaving trails of cryptic symbols in their wake."



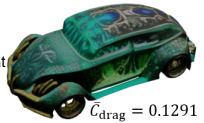
Prompt: "A car in the shape of a colossal, iridescent scarab beetle, its polished chitinous shell reflecting the desert sun, with glowing emerald eyes that serve as headlights and a hidden compartment within its thorax for storing precious cargo."



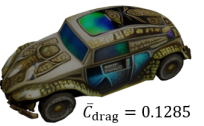
Prompt: "A car in the shape of a colossal, iridescent scarab beetle, its polished obsidian shell reflecting the desert sun, with wheels that are stylized, glowing emerald glyphs, and exhaust pipes that exhale a gentle, perfumed mist, leaving trails of ancient, forgotten languages in their wake."



Prompt: "A car in the shape of a colossal, iridescent scarab beetle, its shell shimmering with fractal patterns, with wheels that are glowing emerald glyphs, and exhaust pipes that exhale a gentle mist, leaving trails of ancient hieroglyphs and golden dust in their wake."



Prompt: "A car in the shape of a colossal, iridescent scarab beetle, its shell shimmering with fractal patterns and reflecting the desert sun, with wheels that are stylized, and exhaust pipes that exhale a gentle mist, leaving trails of ancient hieroglyphs in their wake."



Prompt: "A car in the shape of a colossal, iridescent scarab beetle, its shell shimmering with fractal patterns and polished obsidian, with wheels that are stylized, glowing glyphs, and exhaust pipes that exhale a gentle mist, leaving trails of ancient hieroglyphs in their wake."



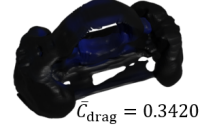
(b) LLM-to-Phy3D

Figure 15: Examples of 3D cars generated with existing Gemini-2.0-Lite and Trellis text-to-3D generative model (Left) and with LLM-to-Phy3D (Right). Note that the lower the aerodynamic drag, the better the physical performance of the generated car.

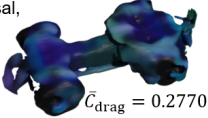
Prompt: "A car in the shape of" and ends with a period, ready for creative car descriptions: A car in the shape of a bioluminescent deep-sea anglerfish, complete with a glowing lure and articulated fins, navigating a neon-drenched cyberpunk cityscape."



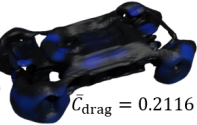
Prompt: "A car in the shape of a colossal, iridescent geode, cracked open to reveal a glowing, crystalline engine block, with wheels crafted from polished obsidian and treads of woven moonlight."



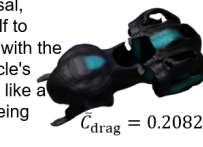
Prompt: "A car in the shape of a colossal, iridescent soap bubble, perpetually shimmering and reflecting distorted cityscapes, with wheels crafted from solidified, swirling nebulae and exhaust pipes that exhale trails of pure, musical sound waves."



Prompt: "A car in the shape of a colossal, iridescent geode, split open to reveal a swirling, crystalline interior, with wheels crafted from polished obsidian and exhaust pipes that exhale shimmering, nebula-like clouds."



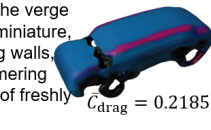
Prompt: "A car in the shape of a colossal, iridescent geode, smoothly sliced in half to reveal a luxurious, velvet-lined interior, with the exposed crystal faces forming the vehicle's exterior, reflecting the vibrant city lights like a thousand tiny prisms and the wheels being replaced by levitating, glowing orbs."



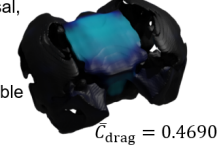
Prompt: "A car in the shape of a colossal, iridescent geode, split open to reveal a swirling vortex of liquid light where the engine should be, with wheels crafted from polished obsidian and glowing, crystalline headlights that pulse with a slow, rhythmic beat."



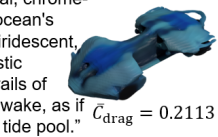
Prompt: "A car in the shape of a colossal, iridescent soap bubble, perpetually on the verge of popping, yet somehow containing a miniature, chrome-plated city within its shimmering walls, with tire treads that leave trails of shimmering stardust, and exhaust fumes that smell of freshly baked cinnamon rolls."



Prompt: "A car in the shape of a colossal, iridescent geode, split open to reveal a swirling, crystalline interior, with wheels crafted from polished obsidian and glowing, ethereal headlights that resemble captured starlight."

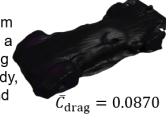


Prompt: "A car in the shape of a colossal, chrome-plated seashell, its curves echoing the ocean's rhythm and its interior shimmering with iridescent, pearl-like seats, with barnacles of futuristic technology clinging to its surface, and trails of bioluminescent light emanating from its wake, as if it's perpetually gliding through a cosmic tide pool."

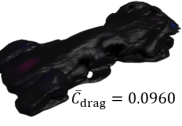


(a) Existing Gemini-2.0-Lite with Shap-E model

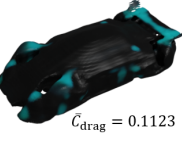
Prompt: "A car in the shape of a colossal, iridescent geode, its segmented body crafted from lustrous obsidian and bioluminescent veins, with a retractable lure-headlight and sharp teeth forming the grill, and sleek, black panels covering the body, with an engine fueled by compressed plasma and an interior crafted from constellations."



Prompt: "A car in the shape of a colossal, iridescent geode, its body crafted from polished obsidian and bioluminescent veins, a retractable lure-headlight and sharp teeth forming the grill, and sleek, black panels covering the body, with an engine fueled by compressed plasma and an interior crafted from constellations."



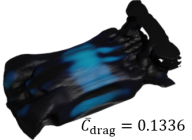
Prompt: "A car in the shape of a colossal, iridescent geode, its segmented body crafted from polished obsidian and bioluminescent veins, a retractable lure-headlight forming the grill, and sleek, black panels covering the car, with an engine fueled by compressed plasma and an interior crafted from constellations."



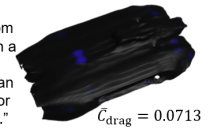
Prompt: "A car in the shape of a colossal geode, its segmented body crafted from polished obsidian and bioluminescent veins, with a retractable lure-headlight and jagged teeth forming the grill, and sleek, black panels covering the body, with an engine fueled by compressed plasma and an interior crafted from constellations."



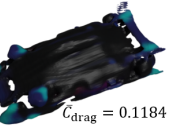
Prompt: "A car in the shape of a colossal, iridescent geode, its segmented body crafted from obsidian and bioluminescent veins, with a retractable lure-headlight extending from the hood, and sleek panels covering the body, with an engine fueled by compressed plasma and an interior crafted from constellations."



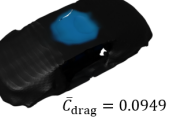
Prompt: "A car in the shape of a colossal, iridescent geode, its segmented body crafted from polished obsidian and bioluminescent veins, with a massive, glowing lure extending from the hood, and sleek, black panels covering the body, with an engine fueled by captured starlight and an interior crafted from polished chrome and constellations."



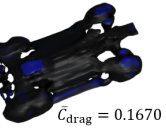
Prompt: "A car in the shape of a colossal, iridescent geode, with a massive, glowing lure extending from the hood, jagged teeth forming the grill, and sleek, obsidian panels covering the body, with an engine fueled by captured starlight and an interior crafted from polished chrome and constellations."



Prompt: "A car in the shape of a bioluminescent geode, with a sleek, black body, split open to reveal a swirling vortex of liquid light, and wheels crafted from polished obsidian and exhaust pipes that exhale trails of sparkling stardust."



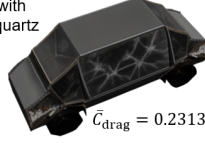
Prompt: "A car in the shape of a colossal, iridescent geode, its segmented body crafted from polished obsidian and bioluminescent veins, with wheels crafted from polished obsidian and exhaust pipes that exhale trails of sparkling stardust."



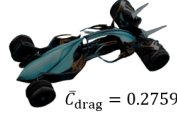
(b) LLM-to-Phy3D

Figure 16: Examples of 3D cars generated with existing Gemini-2.0-Lite and Shap-E text-to-3D generative model (Left) and with LLM-to-Phy3D (Right). Note that the lower the aerodynamic drag, the better the physical performance of the generated car.

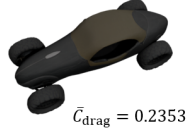
Prompt: "A car in the shape of a crystal, with faceted edges and smooth surfaces like quartz and gemstones."



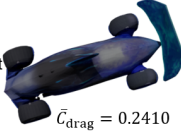
Prompt: "A car in the shape of a symbiotically merging an Origami crane and a suspension bridge, with fluid dynamic lines flowing seamlessly from the sleek metallic hood to the LED light tail fins of the uniquely shaped back, while the wheels are adorned with intricate Art Deco geometric patterns."



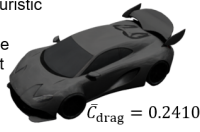
Prompt: "A car in the shape of a serpent, with a body that is a long, winding, open-ended tube, a pair of long, straight front ends, and a pair of side radiators."



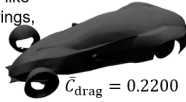
Prompt: "A car in the shape of a sleek, futuristic dolphin leaping through the waves, with a translucent, iridescent body that reflects the surrounding environment, and a tail fin that serves as a dynamic spoiler."



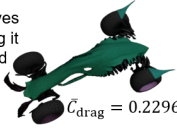
Prompt: "A car in the shape of a sleek, futuristic dolphin leaping through the waves, with a translucent, iridescent body that reflects the surrounding environment, and a tail fin that serves as a dynamic spoiler."



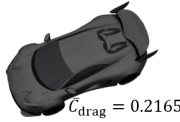
Prompt: "A car in the shape of a sleek, elongated teardrop, with a roof that curves like a whale's back, and doors that open like wings, inspired by the graceful flight of a bird."



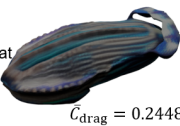
Prompt: "A car in the shape of a graceful seahorse, with a long, flowing bonnet that curves upwards like the animal's neck and tail, making it appear as if it is dancing in motion, smooth and sleek to optimize aerodynamics, the design forms a seamless blend of nature and technology, emphasizing fluidity and grace."



Prompt: "A car in the shape of a majestic, soaring bird, with its body sleek and aerodynamic, and its wings transformed into sweeping aerodynamic surfaces, and its tail feathers morphing into a graceful, elongated rear spoiler."

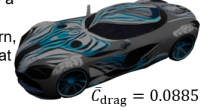


Prompt: "A car in the shape of a sleek, spiral seashell, with its body twisting elegantly from the front to the rear, as if caught in an eternal wave, with a translucent, iridescent surface that shimmers like the sea, and five aerodynamic, fin-like protrusions that act as both decorative elements and functional air vents."



(a) Existing Mistral-3.1-Small with Trellis model

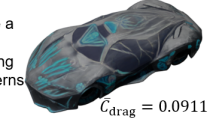
Prompt: "A car in the shape of a sleek, elongated teardrop, with a roof that arcs like a jellyfish's tentacles, and a front grille that resembles a delicate, geometric spiral pattern, adorned with intricate, sweeping patterns that evoke the fluidity of stream currents and the dynamic flow of a kaleidoscope pattern."



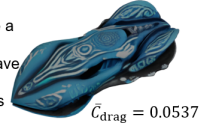
Prompt: "A car in the shape of a sleek, elongated teardrop, with a roof that arcs like a dragonfly's wings, and a front grille that resembles an abstract geometric spider web, adorned with intricate, swirling patterns that evoke the fluidity of air currents and the dynamic flow of a dragonfly's wings."



Prompt: "A car in the shape of a sleek, elongated teardrop, with a roof that arcs like a dragonfly's wings, and a front grille that resembles a delicate, geometric butterfly wing pattern, adorned with intricate, swirling patterns that evoke the fluidity of air currents and the dynamic flow of a whirlpool."



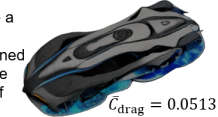
Prompt: "A car in the shape of a sleek, elongated teardrop, with a roof that arcs like a sea dragon's tail, and a front grille that resembles a delicate, geometric seashell wave pattern, adorned with intricate, swirling patterns that evoke the fluidity of air currents and the dynamic flow of Art Deco."



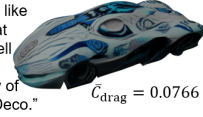
Prompt: "A car in the shape of a sleek, elongated teardrop, with a roof that arcs like a dragonfly's wings, and a front grille that resembles an abstract geometric kaleidoscope pattern, adorned with intricate, swirling patterns that evoke the fluidity of wind currents and the dynamic flow of a whirlpool's flow."



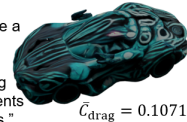
Prompt: "A car in the shape of a sleek, elongated teardrop, with a roof that arcs like a sea dragon's tail, and a front grille that resembles a delicate, geometric spiral, adorned with intricate, swirling patterns that evoke the fluidity of water currents and the elegance of Art Nouveau."



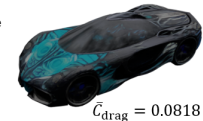
Prompt: "A car in the shape of a sleek, elongated teardrop, with a roof that arcs like a dragonfly's wings, and a front grille that resembles an abstract geometric seashell wave pattern, adorned with intricate, sweeping patterns that evoke the fluidity of water currents and the elegance of Art Deco."



Prompt: "A car in the shape of a sleek, elongated teardrop, with a roof that arcs like a jellyfish's tentacles, and a front grille that resembles an abstract geometric butterfly wing pattern, adorned with intricate, swirling patterns that evoke the fluidity of river currents and the dynamic flow of a dragonfly's wings."



Prompt: "A car in the shape of a sleek, elongated teardrop, with a roof that arcs like a jellyfish's tentacles, and a front grille that resembles a delicate dragonfly's wings, adorned with sweeping patterns that evoke the fluidity of air currents and the dynamic flow of a whirlpool."



(b) LLM-to-Phy3D

Figure 17: Examples of 3D cars generated with existing Mistral-3.1-Small and Trellis text-to-3D generative model (Left) and with LLM-to-Phy3D (Right). Note that the lower the aerodynamic drag, the better the physical performance of the generated car.

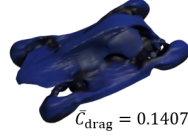
Prompt: "A car in the shape of a sleek, elongated teardrop, with a roof that curves like a gull's wings, and a front grille that mimics the intricate pattern of a honeycomb, and a rear that tapers to a point like an arrowhead."



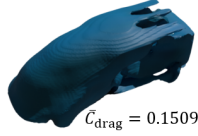
Prompt: "A car in the shape of an abstract origami crane, with fluid, folded panels and its sharp, pointy beak as the front of the vehicle."



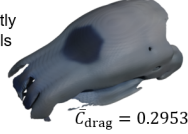
Prompt: "A car in the shape of a majestic, spiraling seashell, with sweeping lines that evoke the grace of a nautilus, and a roof that spirals upwards, evoking a sense of mystery and adventure, and a body that tapers off to the rear of the car, like the tail of a fish."



Prompt: "A car in the shape of a spiraling nautilus shell, with fluid, organic lines that gracefully blend the hood, roof, and trunk, giving the illusion of constant motion, as if caught in a perpetual spin."



Prompt: "A car in the shape of a sleek, spiraling nautilus shell, with the cabin elegantly wrapped around a central column, and wheels that resemble the spiral's final loops."



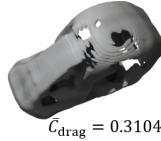
Prompt: "A car in the shape of a giant, metallic dragonfly, with a smooth, aerodynamic body, and wings transformed into sleek, folding doors."



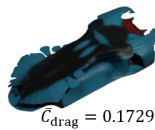
Prompt: "A car in the shape of a spiral seashell, with the wheels acting as the spiral ends, with the windows of the car as the shell's ribbed lines, with the front end of the car as the shell's mouth."



Prompt: "A car in the shape of a spiral seashell, with a body that gracefully curves and twists upwards, mirroring the natural form of a nautilus."



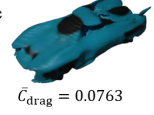
Prompt: "A car in the shape of a sleek, elongated teardrop, inspired by the aerodynamic design of a manta ray, with a roof that curves like the wings of a bird in flight, and a front grille that resembles a stylized, abstract sunburst, and a rear that tapers gracefully like the tail of a comet."



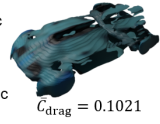
Prompt: "A car in the shape of a sleek, elongated geometric wave seashell, with sweeping, aerodynamic abstract curves that mimic the fluidity of ocean currents and a distinctive, angular front spider web grille that resembles an intricate, stylized geometric flower pattern, inspired by a translucent, abstract spider web dolphin gliding through the ocean."



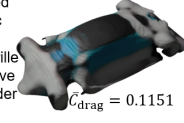
Prompt: "A car in the shape of a sleek, elongated geometric wave flower, with sweeping, aerodynamic dragonfly curves that mimic the fluidity of ocean currents and a distinctive, angular front spider web grille that resembles an intricate, stylized geometric seashell dolphin pattern, inspired by a translucent, abstract wave dolphin gliding through the ocean."



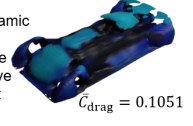
Prompt: "A car in the shape of a sleek, elongated geometric wave flower, with sweeping, aerodynamic dragonfly curves that evoke the fluidity of ocean currents and a distinctive, angular front spider web grille that resembles an intricate, stylized geometric seashell pattern, inspired by a translucent, geometric spider web flower gliding through the ocean."



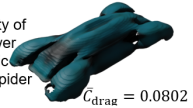
Prompt: "A car in the shape of a sleek, elongated geometric seashell, with sweeping, aerodynamic abstract curves that evoke the fluidity of ocean currents and a distinctive, angular front flower grille that resembles an intricate, stylized Art Deco wave pattern, inspired by a translucent, geometric spider web dolphin gliding through the ocean."



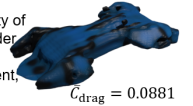
Prompt: "A car in the shape of a sleek, elongated geometric seashell wave, with sweeping, aerodynamic Art Deco curves that evoke the fluidity of ocean currents and a distinctive, angular front flower grille that resembles an intricate, stylized geometric wave jellyfish pattern, inspired by a translucent, abstract spider web flower gliding through the ocean."



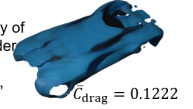
Prompt: "A car in the shape of a sleek, elongated geometric seashell jellyfish, with sweeping, aerodynamic Art Deco curves that evoke the fluidity of ocean currents and a distinctive, angular front flower grille that resembles an intricate, stylized geometric wave pattern, inspired by a translucent, abstract spider web dolphin gliding through the ocean."



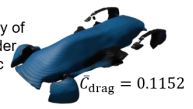
Prompt: "A car in the shape of a sleek, elongated geometric wave dragonfly, with sweeping, aerodynamic Art Deco curves that evoke the fluidity of ocean currents and a distinctive, angular front spider web grille that resembles an intricate, stylized geometric seashell pattern, inspired by a translucent, abstract flower jellyfish gliding through the ocean."



Prompt: "A car in the shape of a sleek, elongated geometric seashell dolphin, with sweeping, aerodynamic Art Deco curves that mimic the fluidity of ocean currents and a distinctive, angular front spider web grille that resembles an intricate, stylized geometric flower pattern, inspired by a translucent, abstract wave jellyfish gliding through the ocean."



Prompt: "A car in the shape of a sleek, elongated geometric seashell dolphin, with sweeping, aerodynamic Art Deco curves that mimic the fluidity of ocean currents and a distinctive, angular front spider web that resembles an intricate, stylized geometric wave pattern, inspired by a translucent, geometric spider web jellyfish gliding through the ocean."



(a) Existing Mistral-3.1-Small with Shap-E model

(b) LLM-to-Phy3D

Figure 18: Examples of 3D cars generated with existing Mistral-3.1-Small and Shap-E text-to-3D generative model (Left) and with LLM-to-Phy3D (Right). Note that the lower the aerodynamic drag, the better the physical performance of the generated car.